NJC

New Journal of Chemistry

A journal for new directions in chemistry

Accepted Manuscript

This article can be cited before page numbers have been issued, to do this please use: A. E. Ramadan, S. Shaban, M. Ibrahim, A. Nassar, S. Sallam, S. El-Harbi and W. Omar, *New J. Chem.*, 2020, DOI: 10.1039/C9NJ06131B.

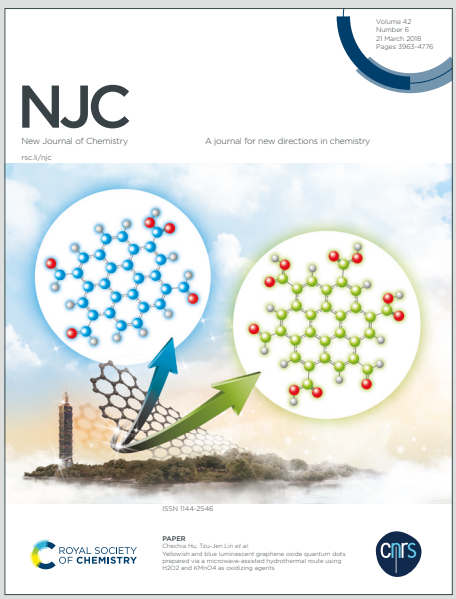

This is an Accepted Manuscript, which has been through the Royal Society of Chemistry peer review process and has been accepted for publication.

Accepted Manuscripts are published online shortly after acceptance, before technical editing, formatting and proof reading. Using this free service, authors can make their results available to the community, in citable form, before we publish the edited article. We will replace this Accepted Manuscript with the edited and formatted Advance Article as soon as it is available.

You can find more information about Accepted Manuscripts in the Information for Authors.

Please note that technical editing may introduce minor changes to the text and/or graphics, which may alter content. The journal's standard Terms & Conditions and the Ethical guidelines still apply. In no event shall the Royal Society of Chemistry be held responsible for any errors or omissions in this Accepted Manuscript or any consequences arising from the use of any information it contains.

View Article Online
DOI: 10.1039/C9NJ06131B

Synthesis and Spectroscopic Characterization of Ternary Copper(II) Complexes Containing Nitrogen and Oxygen Donors as Functional Mimics of Catechol Oxidase and Phenoxazinone Synthase

Abd El-Motaleb. M. Ramadan[a*], Shaban. Y. Shaban[a], Mohamed. M. Ibrahim[a,b], Adel A. Nassar[c], Shehab A. Sallam[d], Sami A. El-Harbi[e], Walid Omar[a]

[a]Department of Chemistry, Faculty of Science, Kafr El-Sheikh University, Kafr El-Sheikh, Egypt
[b]Department of Chemistry, Faculty of Science, Taif University, Taif, Saudi Arabia
[c]Department of Chemistry, Faculty of Science, El-Menuofia University, Egypt
[d]Department of Chemistry, Faculty of Science, Suez Canal University, Ismailia, Egypt
[e]Department of Chemistry, University College in Al-Jamoum, Umm Al-Qura University, Makkah, Saudi Arabia

Abstract

Two ternary copper(II) complexes **1** $[Cu_2Me_4en)_4(EDTA)]$ and **2** $[CuMe_4en)_2(MIDA)]$ containing mixed ligand system of 1,1′,4,4′- tetra methyl ethylenediamine (Me_4en) based (L) and N-methyl iminodiacetic ($MIDAH_2$) (L′) or the ethylene diamine tetra acetic acid ($EDTAH_4$) (L′) were synthesized. Complete structural figuration was achieved by many spectroscopic, electrochemical and magnetic measurements. In addition, spectral data of PXRD with Expo 2014's structural solution software were utilized in the structural illustration of homobinuclear complex **1**. Furthermore, the structural formulation of complex **2** was affirmed by structural analysis of single-crystal X-rays. Square pyramidal stereochemistry is suggested for both the homobinuclear and mononuclear **1** and **2**. The oxidase catalytic activities of complexes **1** and **2** were tested towards a series of catechols and *o*-aminophenol and found to be promising candidates as functional mimics of catechol oxidase and phenoxazinone synthase. Tendency of the studied phenols to oxidize and transform to the oxidation products is correlated with their binding affinity to current complexes and substrates structure. Driving force (λ) or the free energy change, $-\Delta G^{o}$ of the studied oxidation processes were computed from the electrochemical results. The plausible catalytic reactions pathways were suggested in the light of spectral, electrochemical and stopped-follow kinetic measurements.

*Corresponding author: Ramadanss@hotmail.com
33516 Kafr El-Sheikh, Egypt; Tel: 00201273604106; Fax: 0020473215175

View Article Online
DOI: 10.1039/C9NJ06131B

Keywords: Ternary copper(II) complexes, electrochemical, X-ray, catechol oxidase, phenoxazinone synthase, biomimetic, catalytic activity, stopped-follow kinetic

Introduction

Catalytic aerobic oxidation of phenolic compounds leads to formation of biologically significant products like *o*-quinones and *o*-benzoquinone monoimine (*o*-BQMI) [1]. Quinones are of great significance in biological systems; especially due to their capability to undergo redox reactions [2]. Because of its high chemical activity, *o*-quinones perform many vital functions in mammals, animal and plant kingdoms, as well as humans such as antibiotics, defensive secretions, balanid adhesion and pigmentation [2]. Ortho quinones are highly sensitive to nucleophilic addition reactions and this feature makes them as worthy cross - linking agents. The greatest benefit of quinones is the formation of melanin pigment which provides protection for all living organisms from sun damage. Furthermore, melanin in the brain helps in electron transfer processes and in the eyes excited by UV-light to produce tyrosyl radicals, which appear to play a role in visual perception [3].

Related to *o*-quinones is the *o*-benzoquinone monoimine (*o*-BQMI) the precursor for formation of the vital biological component *o*-amino-3H-phenoxazine-3-ones (APX) core [4]. Ortho-amino-3H-phenoxazine-3-ones is the aerobic oxidative dimerization reaction constitute which contained in the final step of the bacterial synthesis of the antibiotic (*Streptomyces antibiotic*), Actinomycin D [4]. Furthermore, *o*-amino-3H-phenoxazine-3-ones chromophore has been proven to be substantial constituent in both xanthommatin and cinnabarin [5]. Clinical trials have proven that the natural product antibiotic Actinomycin D is promising medicine in treatment many critical diseases such as Choriocarcinoma, Wilm's tumors, rhabdomyosarcoma, and Kaposi's sarcoma [5]. In this regard pharmaceutical experiences displayed that these cytotoxic products are potent antineoplastic agents [5].

In the biological systems the aforementioned vital quinones are obtained catalytically by the aerobic oxidation of phenols in presence of the oxidoreductase metalloproteins. Of these native enzymes is the multi-copper containing proteins that include tyrosinase, catechol oxidase and phenoxazinone synthase. This family of copper enzymes is characterized by the capability to reversibly bound molecular oxygen (O_2) at ambient

View Article Online
DOI: 10.1039/C9NJ06131B

conditions. [6]. Tyrosinase and catechol oxidase can catalyze the four electron oxidation of catechols to the corresponding light absorbing *o*-quinones. Tyrosinase catalyzes the hydroxylation of mono phenolic substrates to catechols followed by the aerobic oxidation of the resulting catechols to the corresponding *o*-quinone. On the other hand, catechol oxidase catalyzes only the aerobic oxidation of catechols to *o*-quinone without acting on the monophenols [7]. This is the main difference between these two oxidase copper proteins. In the same context phenoxazinone synthase the oligomeric multicopper oxidase protein catalyzes the aerobic transformation of *o*-aminophenols into the oxidation product *o*-amino-3*H*-phenoxazine-3-ones chromophore through the six-electron oxidative dimerization process.

In the last decades scientists have paid considerable attention for dinucleating ligand systems that have ability to bind two metal cations in the same time [8]. Importance of this subject is owing to existence of the bimetallic heart in a numerous of metalloproteins. Dinucleating ligands were utilized for synthesis abundant number of bimetallic chelates with the aim of mimicking dinuclear native metalloenzymes [9]. More attention is paid to this class of metal chelates for their characteristic magnetic and catalytic properties [10]. In this regard copper(II) complexes are the lighthouse of the bioinorganic models which mimic assorted metalloproteins and also serve as magic catalysts in several catalytic synthetic oxidation reactions [11]. There are a huge number of research articles for dinuclear and mononuclear copper(II) complexes as functional models of catechol oxidase [1,8,12]. On the other hand the available metal complexes as functional mimics of phenoxazinone synthase are few as compared to catechol oxidase [1,13,14].

In seeking a deeper understanding of some chemical and biological oxidation processes, we have resorted to modeling small synthetic molecules to gain valuable insights into these oxidation processes. In this context, we present in this work the synthesis and characterization of two ternary copper(II) complexes as functional models of the active sites of the native copper oxidases catechol oxidase and phenoxazinone synthase. As well the kinetic studies for the catalytic aerobic oxidation of some biologically significant phenols such as catechols and *o*-aminophenol will be carried out.

View Article Online
DOI: 10.1039/C9NJ06131B

2. Experimental

2.1. Chemicals and reagents

The chemicals and reagents used in the present work are of analytical grade. Ligands 1,1′,4,4′-tetramethylethylenediamine (Me_4en), N-methyl iminodiacetic acid (Me-IDA) and ethylenediaminetetraacetic acid (EDTA) were purchased from Merck Chemical Company and used without further refinement. The studied substrates catechol, 4-methyl catechol, 4-nitro catechol, 3,5-di-tert-butyl catechol and *o*-amino phenol were also purchased from Merck Chemical Company and was used as such.

Caution: Perchlorate salts are likely to be explosive and should be handled in small quantities only carefully.

*2.2. Synthesis of copper(II) complexes **1** and **2***

Two and four milimole of aqueous NaOH was added to the N-methyl iminodiacetic acid and ethylenediaminetetraacetic acid respectively in distilled water and the reaction mixture was stirred for 10 minutes. To these mixtures copper(II) salt $(CuClO_4)_2{\cdot}6H_2O$ (1 mmol) in MeOH was slowly added with constant stirring followed by slow addition of 1,1′,4,4′-tetramethylethylenediamine (1.0 mmol) in methanol. After one hour of the constant stirring of the reaction mixtures at room temperature the microcrystalline blue precipitates were formed which were filtered off, washed with MeOH, ether and finally kept in an evacuated desiccator for one week.

2.3. Physical, measurements, catalytic and kinetic experiments were performed as previously described [13a,b,15-16].

3. Results and Discussion

3.1. Synthesis and formulation

The present ternary copper(II) chelates **1** and **2** containing 1,1′,4,4′-tetramethylethylenediamine (Me_4en) based mixed ligands were synthesized facilely at room temperature by mixing the methanolic solutions of copper(II) perchlorate and the sodium salt of the N-methyl iminodiacetic ($MIMDAH_2$) or the ethylenediaminetetraacetic acid followed by the addition of 1,1′,4,4′-tetramethylethylenediamine in an equimolar amounts of the reactants. Copper and chlorine content were determined by EDXRF

View Article Online
DOI: 10.1039/C9NJ06131B

technique while carbon, hydrogen and nitrogen were determined by the usual elemental analysis methods. The suggested molecular formulae given in Table 1 were assigned based on the analytical data and molar conductance measurements. The full structural characterizations were achieved by many spectroscopies, electrochemical and magnetic measurements. In addition, spectral data of PXRD with Expo 2014's structural solution software were utilized in the structural illustration of homobinuclear **1**. Further, the structural formulation of complex **2** was confirmed by X-ray structural analysis for a single crystal.

For the copper(II) complex $[Cu_2L_2L']$ $(NaClO_4)_2$ $2H_2O$ (**1**) the coordinated mixed ligand system (L_2L') in which L′ is the ethylenediaminetetraacetato anion which binds to the two copper(II) ions in a dibasic tridentate pattern per copper(II) ion through the donors sites NO_2. The remaining coordination sites of the penta coordinate conformation are provided by the bidentate based ligand 1,1′,4,4′-tetramethylethylenediamine (L) as depicted in scheme 1. Concerning complex $[CuL_2L'](NaClO_4)_3$ (**2)** the coordinated mixed ligand system (L_2L') in which L is 1,1′,4,4′-tetramethylethylenediamine based ligand coordinates to the copper(II) center in a bidentate pattern via its two nitrogen atoms. On the other hand L′ is the N-methyl iminodiacetato anion which binds to the copper(II) center in a dibasic fashion via the coordination chromophore NO_2.

The solid form of the current copper(II) chelates is microcrystalline shows shades of blue colors (Table 1). The complexes exhibit good solubility in H_2O, DMF, MeOH, EtOH and CH_3CN while in less polar organic solvents a low solubility is observed. Several attempts were made to obtain the single crystal suitable for X-ray structural analysis and only succeeded in the case of complex **2**.

Study the electrolytic conductance of the present copper(II) chelates in the methanolic solution (1×10^{-3}M) at the room temperature (22 °C) confirms the presence of $NaClO_4$ in the crystal lattice of the solid microcrystalline forms of these metal chelates. Based on the analytical data these copper(II) chelates are electrically neutral because they are deprived of the counter anions and consequently a nonelectrolytic behavior is expected in solution. However the electrical conductance measurements indicate their electrolytic nature. This finding was inferred from the electrical conductivity values of 150 and 155 and Ω^{-1} mol^{-1} cm^2 in the case of complexes **1** and **2** respectively which are distinctive to 1:1 electrolytic

View Article Online
DOI: 10.1039/C9NJ06131B

behavior [17]. These detected conductance values are attributed to the electrolytic dissociation of the crystal lattice $NaClO_4$ content as a result of dissolution the microcrystalline solid complexes in MeOH.

Table 1: Molecular formulae, physical prosperities, and elemental analysis data of copper(II) complexes **1** and **2**

Complex	Color	Λ_M $\Omega^{-1}cm^2\ mol^{-1}$	Found (Calcd.) %C	%H	%N	%Cl	%Cu
1.$[Cu_2L_2L']$.$(NaClO_4)_2$ $2H_2O$	Deep Blue	150	28.48 (28.44)	5.19 (5.17)	9.08 (9.05)	7.64 (7.64)	13.69 (13.69)
2.$[CuLL']$.$(NaClO_4)_3$	Blue	155	19.06 (19.07)	3.31 (3.32)	6.08 (6.07)	15.36 (15.38)	9.18 (9.18)

For the two complexes **1** and **2**, L is 1,1′,4,4′- tetra methyl ethylenediamine, for complex **1**, L′ is ethylene diamine tetra acetato and for complex **2**, L′ is N-methyl iminodiacetic acetato

3.2. Mode of bonding

In order to figure out the mode of bonding of the studied ligand systems the FTIR spectral technique was employed. For this purpose IR spectra of the synthesized copper(II) complexes and the free components of the current ligand systems were measured as KBr disk. Assignment of the observed peaks in both high and low frequency regions are listed in Table 2 and the spectral charts are given in the supplementary materials (S1-S6). Spectrum of 1,1′,4,4′- tetra methyl ethylenediamine based ligand displays medium to weak band in the region 2762-2939 cm^{-1} due to the C–N stretching vibration of the tertiary amine [18]. As a result of coordination to copper(II) ion these bands were shifted to 3294 and 3220 cm^{-1} in the spectra of complexes **1** and **2** respectively [19].

Concerning the free N-methyl iminodiacetic acid (NMIDA) and the ethylene diamine tetra acetic acid their spectra exhibit the characteristic frequencies for both tertiary amine and the carboxylate moieties at the regions of 3007-3023 and 1614-1683 cm^{-1} respectively [19]. On complex formation the characteristic peak of C-N is shifted to lower wavenumber in the spectra of the complexes **1** and **2** indicating participation of the

View Article Online
DOI: 10.1039/C9NJ06131B

tertiary amine nitrogen in coordination to copper(II) center [19]. Concerning the carboxylate groups their υ(OH) peak was disappeared in the spectra of the synthesized copper(II) complexes **1** and **2** indicating deprotonation of the COOH group followed by its binding to copper(II) ion via the carboxylate oxygen [20]. In addition the distinctive bands at 1614 - 1683 and 1472 - 1474 cm^{-1} ascribed to $\upsilon_{asym}(COO^{-})$ and $\upsilon_{sym}(COO^{-})$ respectively appeared at 1589 - 1622 and 1498 indicating involvement of (COO^{-}) in coordination to copper(II) center [20]. These spectral features are characteristic to the tridentate dibasic fashion of both the N-methyl iminodiacetato anion ($MIMA^{2-}$) and the ethylene diamine tetra acetato anion ($EDTA^{4-}$) per copper(II) ion. This finding is further supported from the X-ray structural analysis in the case of complex **2**. For both $MIMA^{2-}$ and $EDTA^{4-}$ the unidentate fashion of (COO^{-}) was deduced from the computed value of the frequency difference $\Delta\upsilon(cm^{-1})$; where $\Delta\upsilon = \upsilon_{asym}(COO^{-}) - \upsilon_{sym}(COO^{-})$ =91 - 124 cm^{-1}.

In the low frequency region the newly found stretching vibrations bands within the ranges of 520 - 590 and 485 – 500 cm^{-1} attributed to the ν(M-N) and ν(M-O) respectively are further evidence for the assigned structures given in scheme 1. Based on the analytical data, molar conductance measurements and FTIR spectral investigations the newly synthesized copper(II) complexes **1** and **2** are depicted in scheme 1.

Table 2: FTIR spectra (cm^{-1}) of the ternary copper(II) complexes **1**- **2**

Compound*	ν(OH)	ν(C−N)	$\nu_{as}(COO^{-})$	$\nu_{s}(COO^{-})$	Δν (cm^{-1})	M-N	M-O
$(CH_3)_4en$		2762-2939	-	-	-	-	-
EDTA	3490	3023	1614	1474	-	-	-
1	3106	2915	1589	1498	91	520	500
$MIDAH_2$	3450	3007	1683	1472	-	-	-
2		2887	1622	1498	124	530	485

*$MIDAH_2$ is N-methyl iminodiacetic acid.

View Article Online
DOI: 10.1039/C9NJ06131B

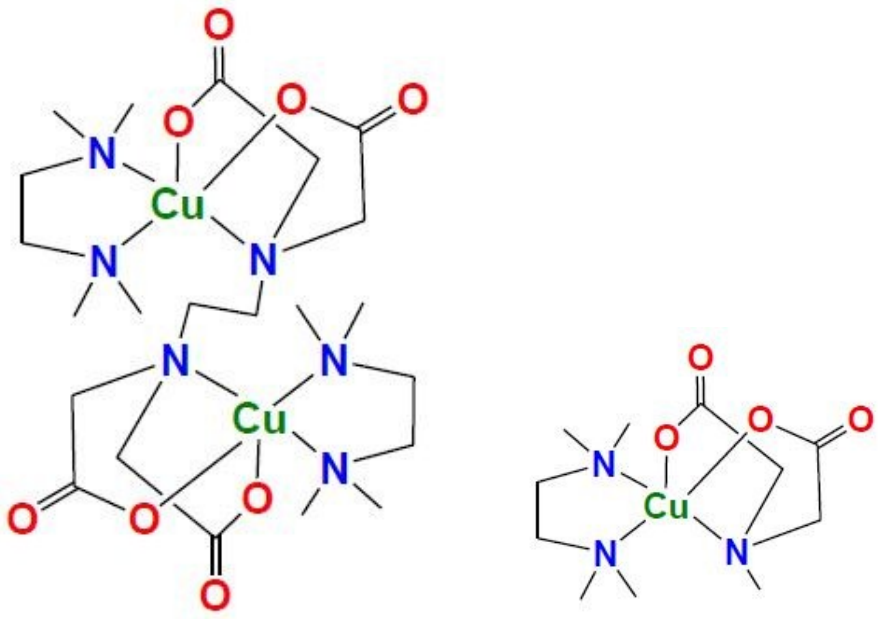

Complex **1** Complex **2**

Scheme 1: Structure of complexes **1** and **2**

3.3. Electronic absorption spectra

Due to lacking of a proper single crystal for X-ray structural analysis in the case of complex **1**, comparative spectral measurements in the UV-Vis region were performed and correlated with complex **2** to explain the structural aspects of **1**. In this regard, the ultraviolet and visible spectra of the present copper(II) chelates were measured as a concentrated solution in MeOH. The recorded spectra as shown in Figure 1 display similar features of the two penta coordinated copper(II) complexes **1** and **2**. On the other hand X-ray structural analysis of **2** demonstrated square pyramidal stereochemistry and therefore we expect square-pyramidal geometry for complex **1**. Further corroboration for these geometrical predictions could be getting from the incoming: i) ESR spectra measurements; ii) the obtained results of the XRD spectral data processing by the structural solutions program - Expo 2014 in the case of complex **1**.

Figure 1 shows that complex **1** and **2** exhibit almost identical band position in the visible region at about 535 nm. Three d-d electronic transitions are usually observed for copper(II) ion in the square-pyramidal environment (C_{4v}) which agree with d_{xz}, $d_{yz} \rightarrow dx^2–y^2$, $d_{xy} \rightarrow dx^2–y^2$ and $dz^2 \rightarrow dx^2–y^2$ transitions [21].

View Article Online
DOI: 10.1039/C9NJ06131B

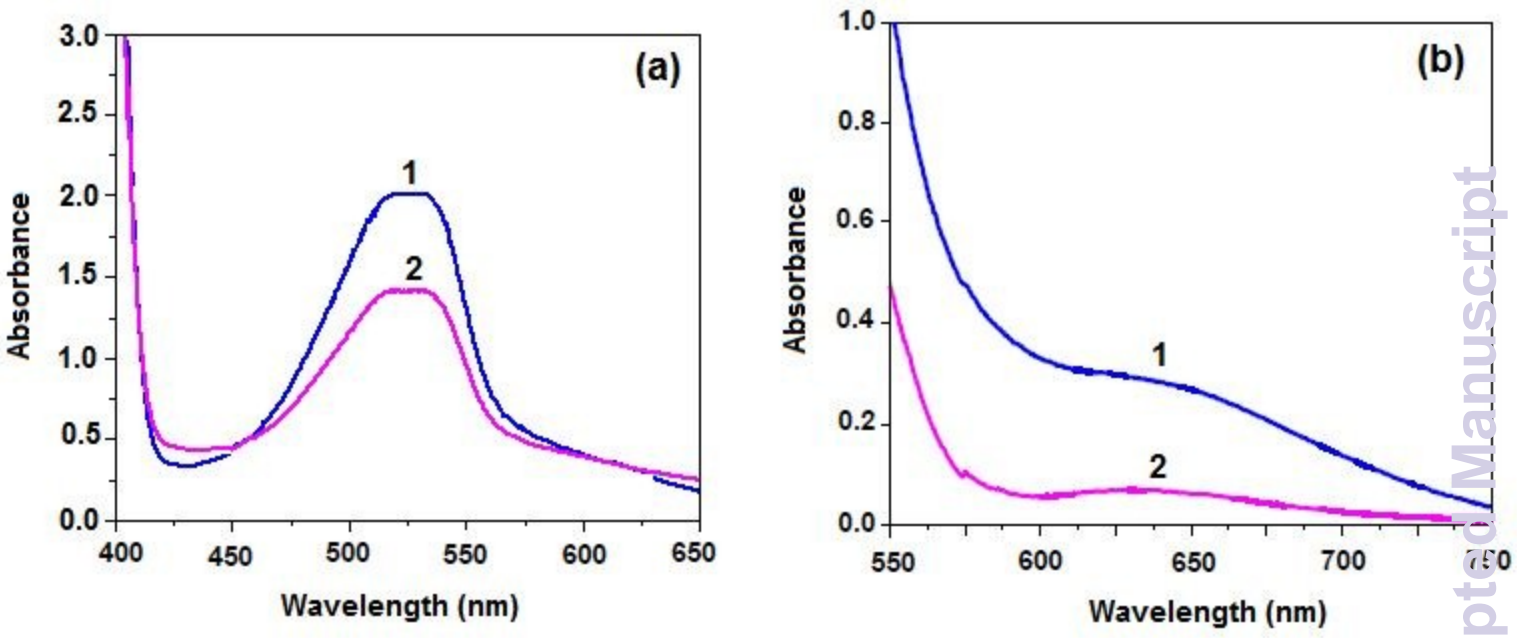

Figure 1(a) and (b): Electronic absorption spectra in methanol for saturated solution of the copper(II) complexes **1** and **2**

The spectra of the current copper(II) complexes display a strong intensity peak at 525 nm may arise from the d-d electronic transitions d_{xz}, $d_{yz} \rightarrow dx^2–y^2$. The other band at ≈ 650 nm is a broad and weak may be assigned to the two superimposed transitions $d_{xy} \rightarrow dx^2–y^2$ and $dz^2 \rightarrow dx^2–y^2$. These spectral features are distinguishing for copper(II) center in the square-pyramidal stereochemistry in a harmony with the previously reported for other penta coordinated copper(II) complexes in a square-pyramidal geometry [22].

3.4. Magnetic moment measurements and EPR spectra

The EPR spectra and magnetic susceptibility measurements are beneficial tools for designate the stereochemistry of the present copper(II) complexes. Accordingly we have measured the magnetic susceptibility of the two copper(II) complexes at room temperature and the computed magnetic moments are given in Table 3.

The observed magnetic moments values of 1.97 and 2.12 BM (Table 3) are slightly greater than the spin only value of 1.73 BM for d^9 configuration in a magnetically non concentrated environment and indicate to magnetic dilute character of the copper(II)

View Article Online
DOI: 10.1039/C9NJ06131B

complexes 1 and 2. This finding ruled out any spin coupling interactions between the neighboring Cu^{II} ions [23] in the powder samples and reflects the monomeric nature of the current newly synthesized copper(II) complexes.

Room temperature powder-EPR measurements of copper(II) complex **1** and **2** have been carried out in the X-band region at scan rate of 1000. The strength of the applied magnetic field is 5000 gauss along with a frequency of 9100 megacycles per second. The EPR-spectral parameters, $g_{\|}$, $g_{\perp}$, g_{av} and G, were determined and listed in Table 3 and the recorded spectra are presented in S7.

The spectra of complexes **1** and **2** are similar and characteristic to the rhombic symmetry (Fig. 3) which yields three different g-values, i. e., $g_x \neq g_y \neq g_z$. The indexed geometrical quotient, (R), where, $R = (g_x - g_y)/(g_y - g_z)$, is beneficial distinguish geometry for the penta coordinated copper(II) complexes [13b]. In the case of $R > 1$ the dz^2 is the ground state but when $R < 1$ the dx^2-y^2 is the ground state which is the most common for copper(II) complexes in the square pyramidal stereochemistry [13b]. The obtained values of R are 0.845 and 0.618 for complexes **1** and **2** respectively which confirm the square pyramidal geometry. As well the numerical value of the indexed geometrical quotient (R) may use as a measure of the geometry distortion of the metal complex. Accordingly the ideal square pyramidal geometry should exhibit R value of zero thus data in Table 3 indicate that complex **1** (R = 0.845) is more distorted than complex **2** (R = 0.618). Anyway, the electronic absorption spectra investigations indicate square pyramidal geometry for the studied copper(II) complexes **1** and **2** and this finding was also corroborated by the EPR study.

The g-values (Table 3) that are estimated from the relation: $g_{av} = 1/3(g_{\|} + 2g_{\perp})$ refer to the predominant covalence in the binding of the coordinated ligand system to copper(II) ion [24]. In the same vein, the EPR parameter (G) that measures the coupling of adjacent spinning centers in the polycrystalline samples was calculated from the relation [25]: $G = (g_{\|} - 2)/(g_{\perp} - 2)$. The computed G-values, 8.974 and 5.774, for complexes **1** and **2** respectively are greater than 4 excluded any spin – spin coupling between the adjacent copper(II) centers in the solid complexes [26] in a consistence with the aforementioned for the magnetic moment values (Table 3).

View Article Online
DOI: 10.1039/C9NJ06131B

Table 3: EPR spectral parameters and magnetic moments of copper(II) complexes **1-2**

Complex*	g_x ($g_{\|}$)	g_y	g_z	($g_{\perp}$)	g_{av}	G	R	μ_{eff}
1	2.179	2.086	1.976	2.031	2.080	5.774	0.845	2.08
2	2.175	2.089	1.950	2.019	2.061	8.974	0.618	1.97

*Complexes details are as listed in Table 1.

3.5. Powder X-ray Diffraction

Nowadays, powder X-ray diffraction (PXRD) along with an appropriate computational study is a scientific technique for full structural determination of low molecular mass polycrystalline materials such as organic, organometallic and metal complexes [27]. Many trials were carried out to obtain a suitable single crystal for structure determination of the copper(II) complexes which succeeded only in the case of complex **2**. Accordingly, the XRD measurements were performed for appropriate microcrystalline sample of the copper(II) chelates **1** and the resulting XRD patterns are given in Figure 2.

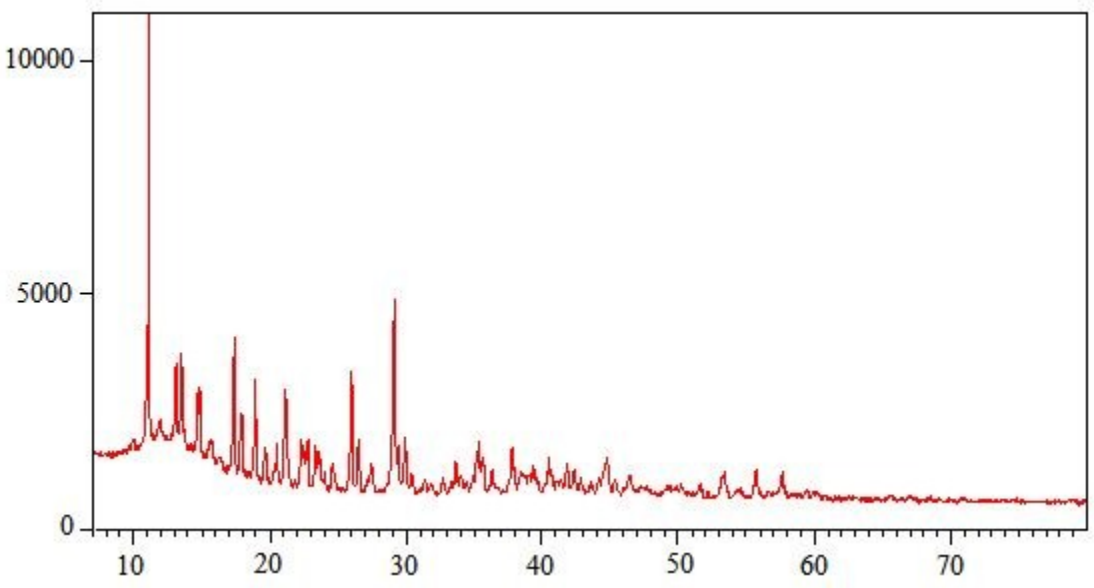

Figure 2 The powder XRD pattern of the homobinuclear copper(II) complex **1**

View Article Online
DOI: 10.1039/C9NJ06131B

The quality of fit between the experimental and the calculated PXRD patterns in the final Rietveld refinement that displayed in Figure 3 provides strong validation of the crystal structure of the examined complex **1**. The Rietveld methodology is a computational treatment of the powder X-ray diffraction data that allows precise structure determinant of the metal complex. In this context the computer program Expo 2014 was utilized to perform all the proceedings of the crystal structure solution process from the PXRD data by the Rietveld technique [28].

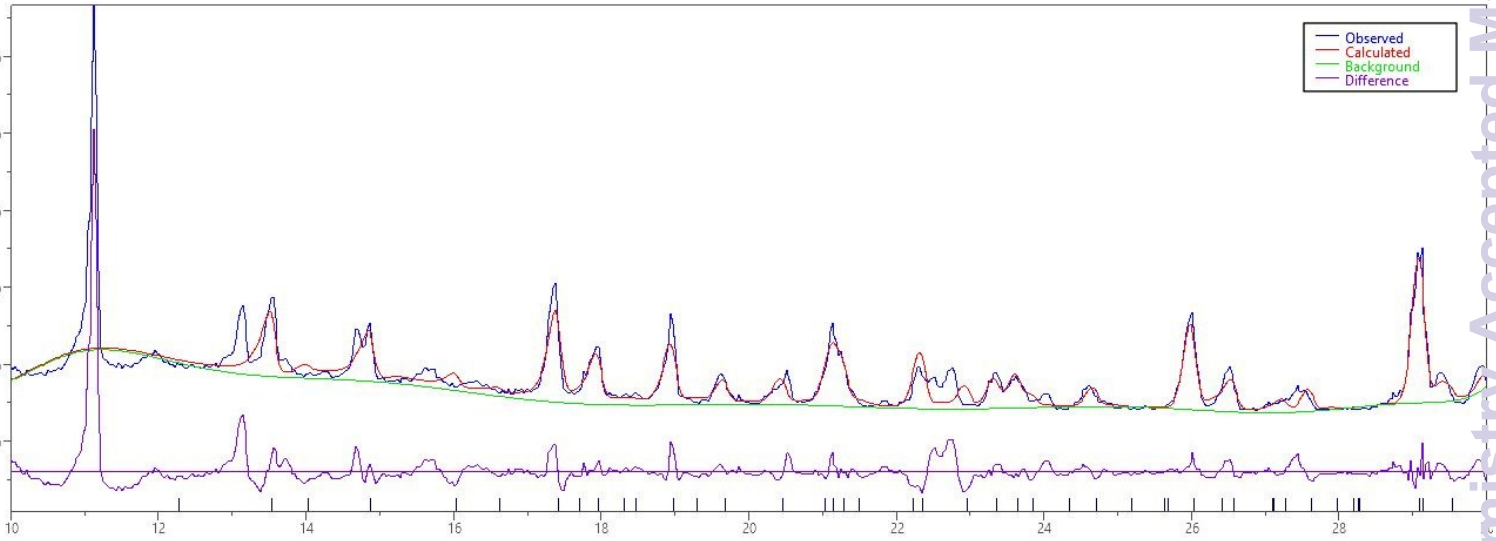

Figure 3: The quality of fit between the experimental powder XRD pattern of complex **1** and the calculated data in the final Rietveld refinement

Table 4 contains the crystallographic data a while selected bond angles and bond length are listed in Tables 5 and 6 respectively. The data in Table 4 showed that complex **1** crystallizes in the monoclinic space group P 1 21 1 with the unit cell dimensions, a =14.34426 Å, b = 12.96501 Å, c = 5.50817 Å, $\alpha = 90°$, $\beta = 95.293°$ and $\gamma = 90°$.

View Article Online
DOI: 10.1039/C9NJ06131B

Table 4: Crystallographic data of the homobinuclear copper(II) complex **1**

Complex (1) $[Cu_2L_2L'](NaClO_4)_2\ 2H_2O$	
Empirical formula	$Cu_2C_{22}H_{48}N_6O_{18}\ Na_2Cl_2$
Formula weight	928.14
T (K)	295
λ (Å)	1.529040
Crystal system	Monoclinic
Space group	P 1 21 1
Centro symmetry	Centric
Space Group Number	4
Unite cell dimensions:	
a (Å)	14.34426
b (Å)	12.96501
c (Å)	5.50817
α (°)	90
β (°)	95.293
γ (°)	90
Cell volume ($Å^3$)	1020.01
Volume per atom ($Å^3$)	51.00
Calculated density (g/cm^3)	1.43
θ range for data collection (°)	10.025 - 30.031
Total reflection	677
Rietveld results:	
Rp	12.383
Rwp	18.953
R-Bragg	6.374
R-F	4.329

View Article Online
DOI: 10.1039/C9NJ06131B

Figure 4 illustrates the optimum structure of complex **1** which has the molecular formula $[(Cu_2L_2L')]$. L′ is the hexadentate ligand (EDTA) and L is the bidentate nitrogen base, 1,1′,4,4′-tetra methyl ethylenediamine.

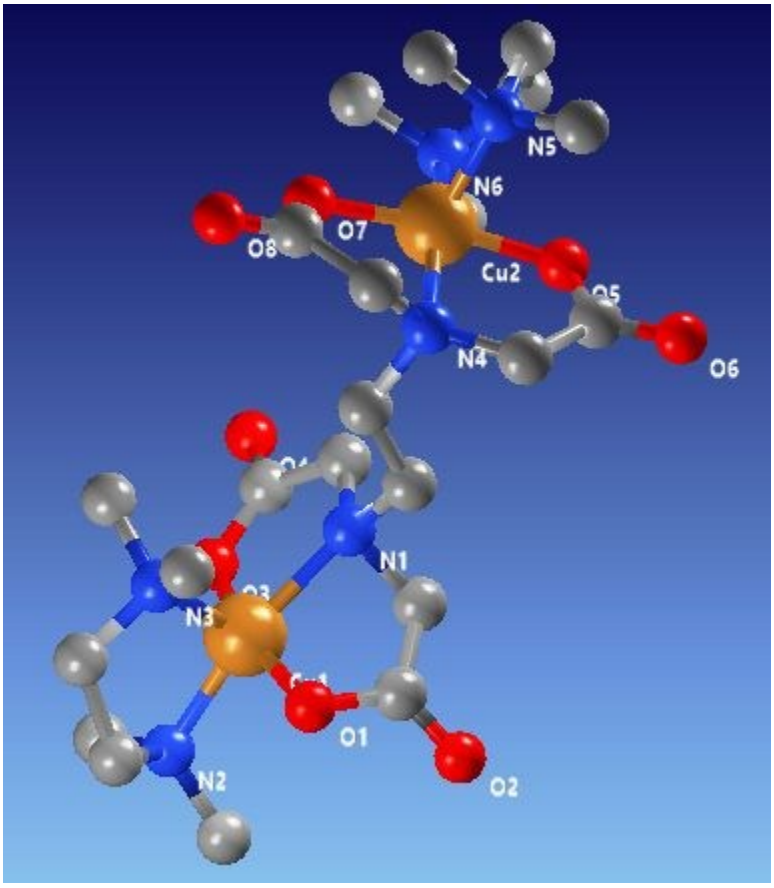

Figure 4: The optimized structure of the homobinuclear copper(II) complex **1**

The coordination chromophore of the present mixed ligand system per copper(II) ion is N_3O which occupies the equatorial plane of the square pyramidal structure while the oxygen atom of the acetato portion of the non-protonated EDTA compartment exists in the apical position. To identify the stereochemistry of the inspected five coordinated copper(II) chelate **1** the geometrical index τ was determined from the relation $\tau = (\beta-\alpha)/60$; where α and β being the two largest angles around the copper(II) center. It has been reported that for the penta-coordinated copper(II) complexes if τ equals zero the hybridization of the copper(II) ion is dsp^3 (d is dx^2-y^2) of the perfect square pyramidal geometry while if τ is one the corresponding geometry is perfect trigonal-bipyramidal

View Article Online
DOI: 10.1039/C9NJ06131B

[29]. The determined values of τ are 0.0920 and 0.0917 for (Cu1) and (Cu2) respectively which demonstrate the distorted square pyramidal stereochemistry. This structural formulation based on the PXRD crystallographic analysis is roughly consistent with the current spectral guides to determine the final structure of **1**.

As shown in Table 5 the bond distances (Cu-N) or (Cu-O) of both EDTA compartment and the nitrogen base, 1,1′,4,4′- tetra methyl ethylenediamine are in the usual values [13c, 22b, 30]. Table 5 shows that the angles of the bond around Cu^{II} centers in the equatorial and apical regions are almost in agreement with those reported for similar copper(II) complexes [13c, 22b, 30].

Table 5: Selected bond length (Å) of the homobinuclear copper(II) complex **1**

N1 − Cu1	2.09467	N4 − Cu2	1.98737
Cu1 − O1	1.82011	Cu2 − O5	1.88153
Cu1 − O3	1.84752	Cu2 − O7	1.87240
N2 − Cu1	1.95729	N5 − Cu2	2.06104
N3 − Cu1	1.99603	N6 − Cu2	1.90816

View Article Online
DOI: 10.1039/C9NJ06131B

Table 6: Selected bond angles (°) of the homobinuclear copper(II) complex **1**

Type	Angle	Type	Angle
C2-N1-Cu1	85.96	C12-N4-Cu2	108.76
C4-N1-Cu1	107.72	C14-N4-Cu2	109.78
Cu1-N1-C11	143.10	C16-N4-Cu2	104.59
N1-Cu1-O1	85.61	N4-Cu2-O5	86.89
N1-Cu1-O3	85.77	N4-Cu2-O7	83.28
N1-Cu1-N2	169.01	N4-Cu2-N5	101.10
N1-Cu1-N3	93.95	N4-Cu2-N6	164.63
C1-O1-Cu1	100.27	C13-O5-Cu	111.73
O1-Cu1-O3	163.49	O5-Cu2-O7	170.13
O1-Cu1-N2	86.51	O5-Cu2-N5	84.18
O1-Cu1-N3	90.91	O7-Cu2-N6	88.04
C3-O3-Cu1	115.43	C15-O7-Cu2	109.75
O3-Cu1-N2	99.91	O7-Cu2-N5	96.85
O3-Cu1-N3	103.72	O7-Cu2-N6	101.69
C5-N2-Cu1	101.20	C17-N5-Cu2	101.69
C6-N3-Cu1	101.76	C18-N6-Cu2	103.74
C9-N2-Cu1	113.18	C21-N5-Cu2	113.57
C10-N2-Cu1	114.78	C22-N5-Cu2	124.46
N2-Cu1-N3	93.81	N5-Cu2-N6	92.80
C7-N3-Cu1	110.35	C19-N6-Cu2	111.18
C8-N3-Cu1	122.75	C20-N6-Cu2	110.80

*3.6. Description of the crystal structure of complex **2***

The final figuration of the ternary copper(II) complex **2** was realized by conducting a structural X-ray analysis of the appropriate blue crystal. The suitable crystal was obtained by the slow evaporation of the methanolic solution of complex 2 at room temperature. The crystalline data are shown in Table 7 where the orthorhombic crystalline system of the space group Pbca is reported and the ORTEP scenery of the asymmetric unit is displayed in Figure 5.

View Article Online
DOI: 10.1039/C9NJ06131B

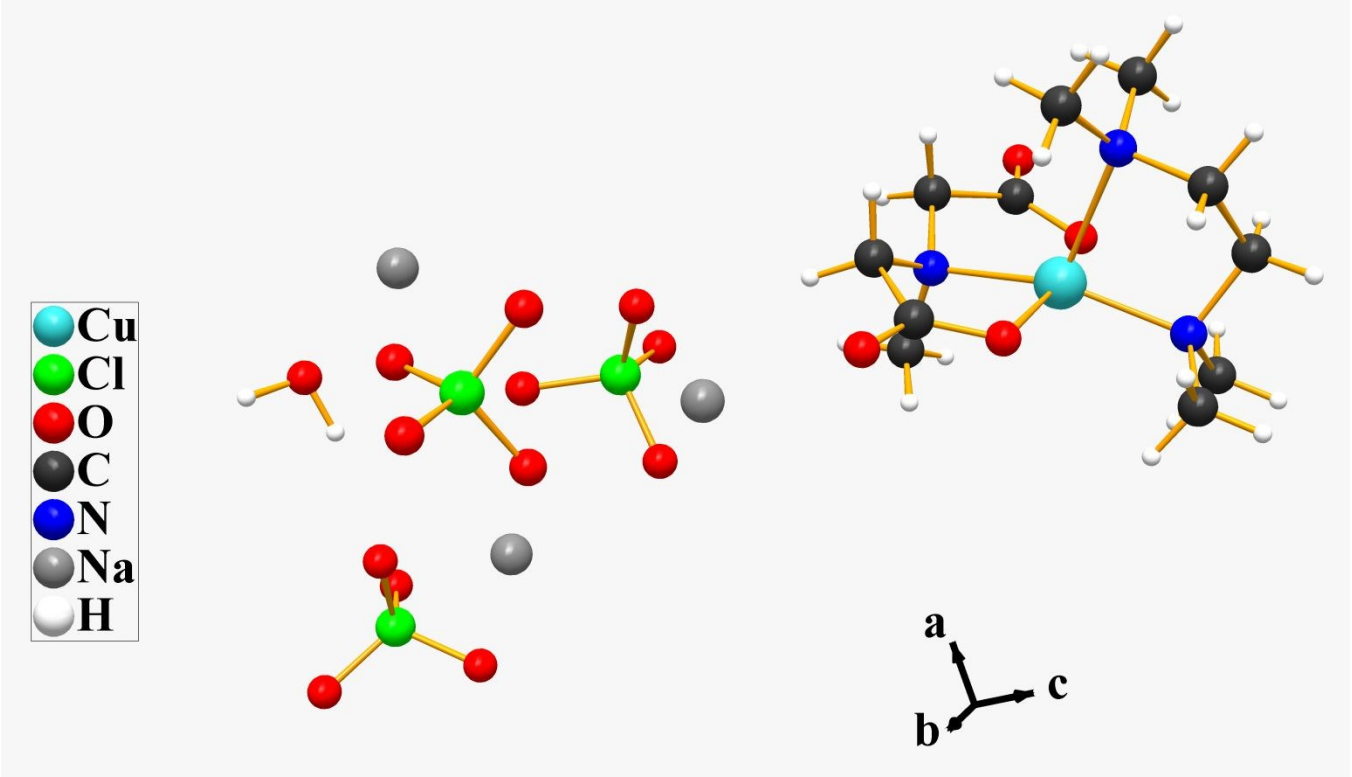

Figure 5: Presentation of the single crystal X-ray structure of copper(II) complex **2**, showing the labeling scheme of non-hydrogen atoms

Tables 8 and 9 report representative bond angles, and bond distances around copper(II) ion. The stereochemistry of the inspected copper(II) complex **2** is proved based on the determined value of the geometrical index τ. The determined τ-value of 0.05 indicates that it is better to describe the stereochemistry of copper(II) complex, **2**, as a slightly distorted square pyramid.

The coordination polyhedron around the copper center shows that the equatorial plane is occupied by both the nitrogen donors of the two tertiary nitrogen atoms of the 1,1′,4,4′-tetra methyl ethylenediamine compartment in addition to the N-methyl tertiary amine nitrogen donor and one of the oxygen atoms of the carboxylate moiety of the coordinated N-methyl iminodiacetic acid. On the other hand the apical position is occupied by the iminodiacetic oxygen (O1) in the square pyramidal conformation. Data in Tables 8 and 9 demonstrate that the bond distances between the copper center and the oxygen and nitrogen donors are in the normal values [13c, 30, 31]. As well as the values of the bond angels around the central copper(II) ion are characteristic to the proven current stereochemistry.

View Article Online
DOI: 10.1039/C9NJ06131B

Table 7: Crystallographic data and structure refinement for complex **2**

Empirical formula	$C_{11}\ H_{23}\ Cl_3\ Cu\ N_3\ Na_3\ O_{16}$
Formula weight	692.07
Temperature [K]	150(2)
Wavelength [Å]	0.71073
Crystal system	Orthorhombic
Crystal color	Blue
Crystal size [mm^3]	0.160 x 0.060 x 0.040
Space group	*Pbca*
Volume [$Å^3$],	5057.0(18), 2
Z	8
Unit cell dimensions [Å; °]	a = 8.3550(17); α = 90
	b =19.633(4); β= 90
	c = 30.829(6) ; γ = 90
Density(calc.) [g/cm^3]	1.866
Absorption coefficient [mm^{-1}]	1.315
F(000)	2888
Theta range for data collection [°]	1.321 to 25.755°
Index ranges of *h, k, l*	10<=h<=9, -23<=k<=23, -37<=l<=35
Refinement method	Full-matrix least-squares on F^2
Reflections collected	33098
Independent reflections	4777 [R(int) = 0.0831]
Completeness to theta	25.000° 100.0 %
Data /restraints / parameters	4777 / 3 / 356
Goodness-of-fit on F^2	0.993
Final R indices [I > 2 sigma(I)]	R1 = 0.0384, wR2 = 0.0904
R indices (all data)	R1 = 0.0678, wR2 = 0.1073
Extinction coefficient	n/a
Largest diff. peak [$e.Å^{-3}$] and hole	0.447 and -0.580

View Article Online
DOI: 10.1039/C9NJ06131B

Table 8: Selected bond lengths [Å] of complex **2**

Bond lengths [Å]	
Cu(1)-O(1)	1.981(3)
Cu(1)-O(3)	1.983(3)
Cu(1)-N(3)	1.994(3)
Cu(1)-N(2)	2.018(3)
Cu(1)-N(1)	2.314(3)

Table 9: Selected bond angles [º] of complex **2**

Bond angles [º]	
O(1)-Cu(1)-O(3)	164.75(10)
O(1)-Cu(1)-N(3)	82.83(11)
O(3)-Cu(1)-N(3)	82.59(11)
O(1)-Cu(1)-N(2)	97.19(11)
O(3)-Cu(1)-N(2)	95.47(11)
N(3)-Cu(1)-N(2)	163.23(13)
O(1)-Cu(1)-N(1)	96.26(11)
O(3)-Cu(1)-N(1)	93.19(11)
N(3)-Cu(1)-N(1)	111.28(12)
N(2)-Cu(1)-N(1)	85.43(12)
Cu(1)-O(1)-Na(3)1	157.72(13)
Cu(1)-O(3)-Na(2)2	162.75(13)
C(7)-N(1)-Cu(1)	115.5(2)
C(8)-N(1)-Cu(1)	98.4(2)
C(6)-N(1)-Cu(1)	114.1(2)
C(11)-N(2)-Cu(1)	112.9(2)
C(10)-N(2)-Cu(1)	110.4(2)
C(2)-N(3)-Cu(1)	107.2(2)
C(3)-N(3)-Cu(1)	105.6(2)
C(5)-N(3)-Cu(1)	107.9(2)

View Article Online
DOI: 10.1039/C9NJ06131B

3.7. Electrochemical studies

All the reported studies for the oxidation of catechols or *o*-aminophenol catalyzed by copper(II) oxidase models or native copper proteins demonstrated the reduction of copper(II) to copper(I) by the concerned phenol. This is followed by oxidation of the generated monovalent copper by the atmospheric oxygen during the catalytic aerobic oxidation cycle. Accordingly the redox potentials for both complexes **1**, **2** and the studied substrates is a key master for the current catalytic oxidation processes.

The electrochemical behavior of complexes **1** and **2** at a carbon paste electrode was studied by using the cyclic voltammetry technique in phosphate buffer of pH value of 7.0 in a potential range from -1.2 to +1.2 V (vs. Ag/AgCl) using a potential scan rate of 50 mVs^{-1}. The methanolic solutions of 1×10^{-3} M of the studied complexes **1** and **2** were used for performing the present cyclic voltammetric measurements. The cyclic voltammograms of both complexes **1** and **2** showed a quasi-reversible systems and well - oxidation peaks (E_{pa}) were appeared at + 0.0 V while the cathodic peaks (E_{pc}) were appeared between -0.33 and -0.35 V (Figure 6 and S8).

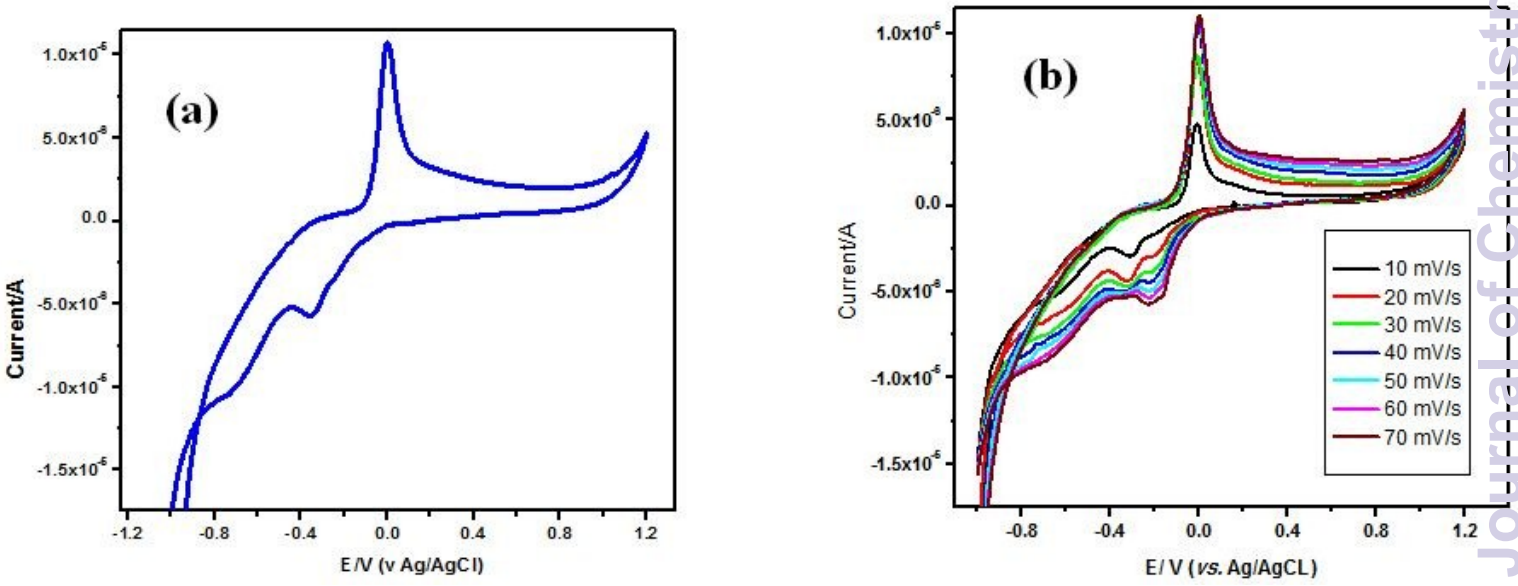

Fig 6: (a) Cyclic voltammogram for complex **1** at CPE at phosphate buffer pH 7 using scan rate of 50 mV/s; (b) Effect of scan rate on the peak current height of 1×10^{-3} M complex **1** using cyclic voltammetry at CPE at phosphate buffer pH 7

The separation of the anodic and cathodic peak potentials (ΔE) was found to be lower than 0.35 and 0.33 V for complexes **1** and **2** respectively (Table 10). The formal potential

View Article Online
DOI: 10.1039/C9NJ06131B

$E_{1/2}$ was taken as the average of E_{pc} and E_{pa} which is found to be + 0.175 and + 0.165 V in the case of **1** and **2** respectively.

The detected redox peaks of cyclic voltammograms are due to the reversible reduction and oxidation behavior of Cu(II)/Cu(I) couple. Subsequently the redox behavior of the current oxidase models can be summarized in scheme 2. In addition to the quasi-reversible system, one cathodic broad peak was appeared at more negative value (-0.73V). The effect of scan rate on the peak currents was examined at different scan rate values which extended from 10 to 70 mV s^{-1}. For both complexes **1** and **2** as the scan rate increases both the anodic and cathodic peak current also increases (Figure 6 and S8).

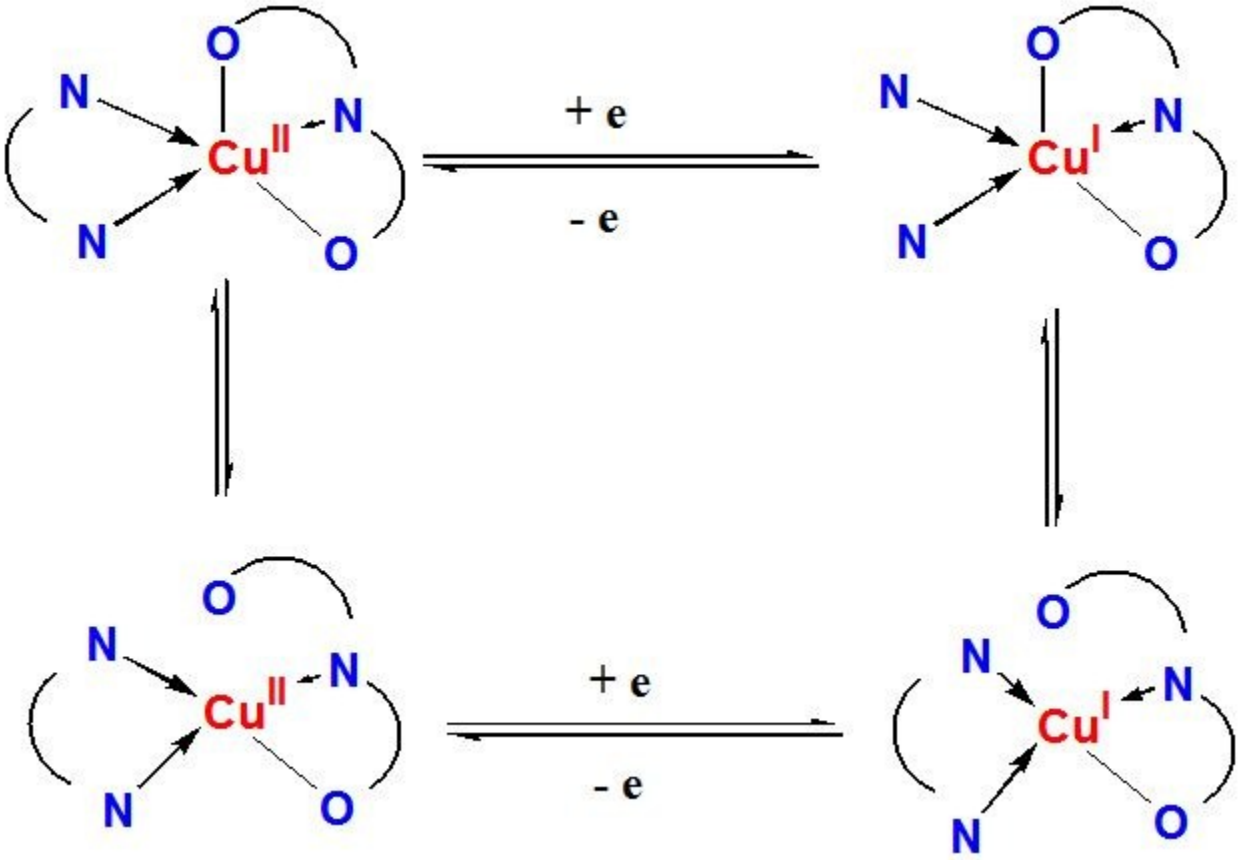

Scheme 2: The square scheme for the observed cyclic voltammograms of copper(II) complexes **1** and **2**

View Article Online
DOI: 10.1039/C9NJ06131B

The electrochemical behavior of 3,5 $DTBCH_2$ as a representative of the studied catechols, was also examined at a carbon paste electrode in a phosphate buffer of pH value of 7. The applied potential range is from -1.0 to +1.5 V (vs. Ag/AgCl) at the potential scan rate of 50 mVs^{-1}. The cyclic voltammogram for 1×10^{-3} M 3,5 $DTBCH_2$ showed well-defined anodic peak current (E_{pa}) at + 0.34V and one cathodic peak (E_{pc}) at -0.1 (S9). The oxidation reaction of 3,5 $DTBCH_2$ is illustrated in reaction 1, where 3,5-$DTBCH_2$ is oxidized to the corresponding light absorbing 3,5-DTBQ [32]. The electrochemical oxidation product 3,5-DTBQ was extracted by CH_2Cl_2 and its spectrum was measured which exhibited the distinctive peak of quinone at 400 nm.

In the same regard the electrochemical behavior of *o*-aminophenol at a carbon paste electrode was examined using phosphate buffer of pH value of 9.5 in a potential range from -1.0 to +1.5 V (*vs.* Ag/AgCl) using a potential scan rate of 50 mVs^{-1}. The cyclic voltammogram for 1×10^{-3} M *o*-APH_3 displays well-defined anodic peak current (E_{pa}) at + 0.36V and one cathodic peak (E_{pc}) at -0.62 (S10). Oxidation of *o*-APH_3 leads to formation of *o*-benzoquinone monoimine (*o*-BQMI) (reaction 4) the precursor for production of *o*-amino-3*H*-phenoxazine-3-ones (APX) [33]. After the electrochemical oxidation of *o*-APH_3 the oxidation product was extracted by CH_2Cl_2. The extracted product was designated as *o*-aminophenoxazin-3-one (APX) based on TLC analysis and comparison with an authentic sample of APX prepared by chemical oxidation of *o*-APH_3.

Table 10: Electrochemical data (mV) of copper(II) complexes **1**, **2**, 3,5-$DTBCH_2$ and *o*-APH_3

Complex/substrate	E_{pc}	E_{Pa}	ΔE_p	$E_{1/2}$
1.[CuL_2 H_2O].Cl_2	− 350	0.00	350	175
2.[CuLL' Cl].H_2O	− 330	0.00	330	165
3,5-$DTBCH_2$	− 100	340	444	120
o-APH_3	− 620	360	980	− 130

View Article Online
DOI: 10.1039/C9NJ06131B

3.8. Catalytic oxidation of biologically significant phenols

The current copper(II) complexes were synthesized with the aim of the functional mimicking of the multicopper proteins catechol oxidase and phenoxazinone synthase in the aerobic catalytic oxidation of various phenols to the corresponding *o*-quinone. Catechol oxidase catalyzes the aerobic transformation of catechol to *o*-quinone via four electrons oxidation of catechol or its derivatives with concomitant reduction of O_2 to two H_2O as a by product as depicted in reaction 1.

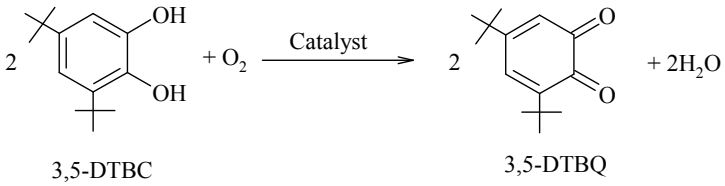

3,5-DTBC 3,5-DTBQ (1)

The reaction catalyzed by the other copper(II) enzyme phenoxazinone synthase is a six-electron oxidation of *o*-aminophenol to *o*-amino-3*H*-phenoxazine-3-one which commonly known as phenoxazinone chromophore (APX) with formation of water as shown in reaction 2.

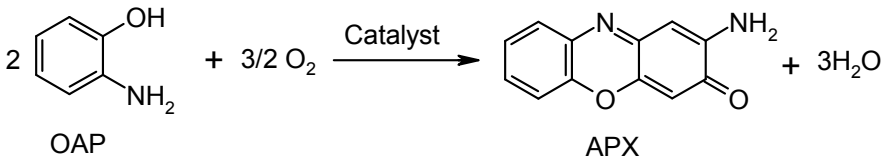

OAP APX (2)

Within the framework of the current study, five phenols (Scheme 3) were studied to investigate the effect of phenol substituents on the catalytic efficiency of the copper(II) complexes under study.

View Article Online
DOI: 10.1039/C9NJ06131B

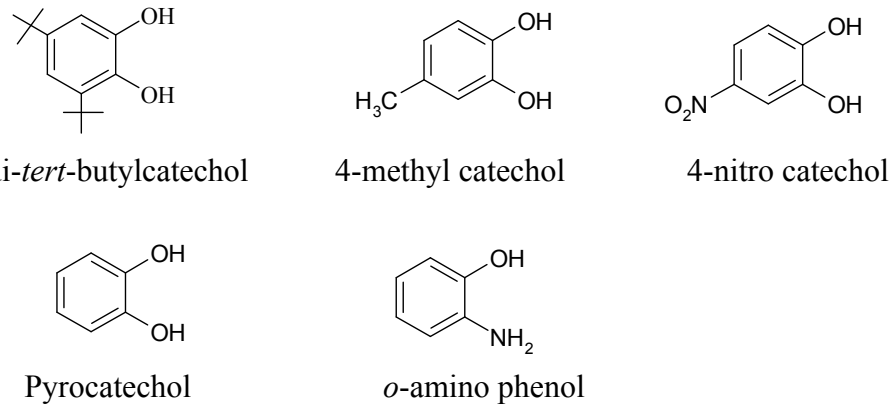

Scheme 3: Structure of the current studied phenols

Study the catalytic oxidation reactions were performed in methanol by mixing the catalyst solution (1×10^{-4}M) with the particular phenol solution (1×10^{-2}M). Oxidation products formation was monitored spectrophotometrically at the wavelengths of 400 and 433 nm distinctive to 3,5-DTBQ and APX respectively. After 24 hours from the beginning of the oxidation reaction, spectral monitoring showed formation of a single oxidation product excluding further oxidative cleavage of 3,5-DTBQ or APX.

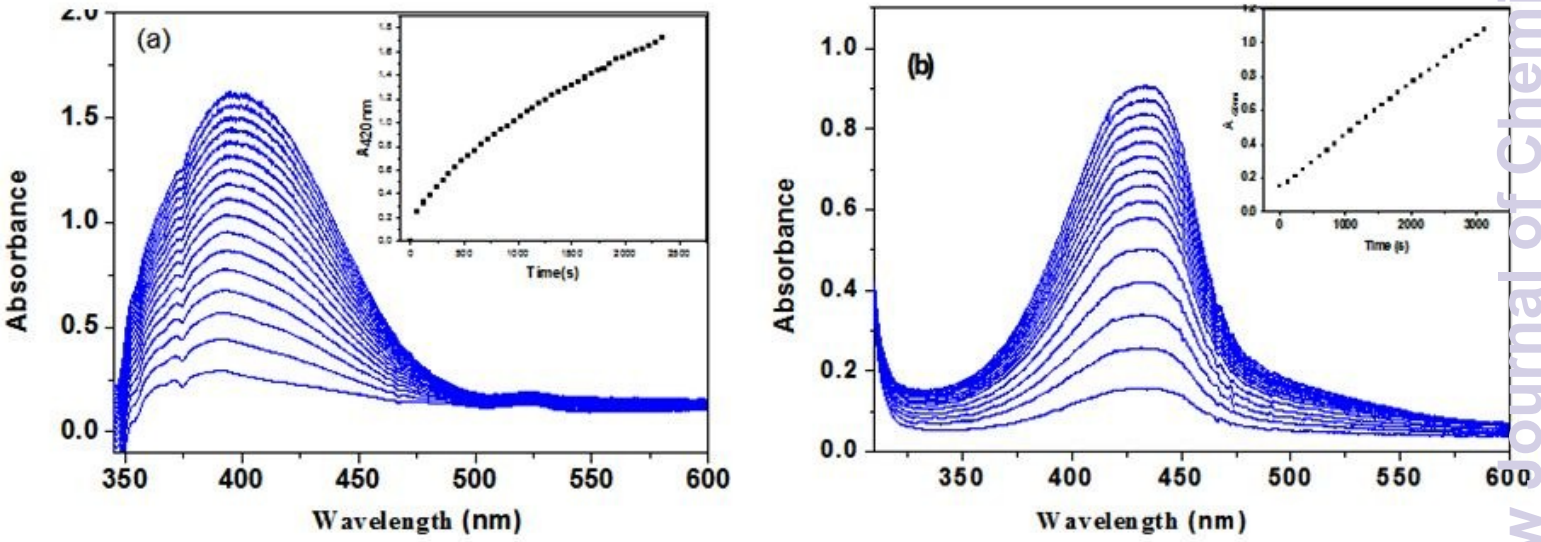

Fig. 7: UV/Vis spectral changes recorded for the catalytic oxidation reaction of both (a) 3,5-DTBCH$_2$ and (b) *o*-APH$_3$ at concentration of (10^{-2} M) in MeOH at 296 K in presence complex **1** (10^{-4} M). Inset shows the course of the absorbance at 400 for (a) and 433 nm for (b) verses time in second.

View Article Online
DOI: 10.1039/C9NJ06131B

Figure 7 shows peak growing of 3,5-DTBQ and APX in presence of complex **1** as a representative spectral profile of the studied catalytic reactions. The substrates being studied are pyrocatechol ($CatH_2$), 3,5-di-*tert*-butylcatechol (3,5-$DTBCH_2$), 4-methyl-catechol (4-Me-$CatH_2$), 4-nitro-catechol (4-NO_2-$CatH_2$) in addition to *o*-aminophenol (*o*-APH_3).

To confirm the catalytic activity of the studied copper(II) complexes, a typical catalytic experiment was performed in the absence of the catalyst. The resulting amount of oxidation product can be neglected when compared to that produced in the presence of the catalyst.

Kinetic investigations

The kinetic measurements were performed using the stopped-flow instrument and the kinetic details showed that in presence of catalyst aerobic oxidation of the current phenols takes place via the formation of binary [substrate-catalyst] and ternary [substrate-catalyst-O_2] intermediates. Accordingly the whole oxidation process can be represented in the reactions 3 and 4 for both 3,5-$DTBCH_2$ and *o*-APH_3 as representative substrates.

$$2\,[Cu^{II}LL'X] + 3,5\text{-DTBC} \underset{k_{-1}}{\overset{k_1}{\rightleftharpoons}} [Cu^{II}LL')_2\text{-}3,5\text{-DTBC}] \xrightarrow[k_2]{O_2} 3,5\text{-DTBQ} + H_2O_2 \qquad (3)$$

$$[Cu^{II}LL'X] + o\text{-}APH_3 \underset{k_{-1}}{\overset{k_1}{\rightleftharpoons}} [(Cu^{II}LL')\text{-}o\text{-}APH_2] \xrightarrow[k_2]{O_2} \text{(}o\text{-BQMI)} + H_2O_2 \qquad (4)$$

It is worth mention that earlier studies [33,5] displayed that *o*-benzoquinone monoimine (*o*-BQMI) is the precursor to APX formation which converts to the final product *o*-amino-3*H*-phenoxazine-3-ones (APX) via further uncatalyzed reactions.

Figure 8 shows that the kinetics trace of 3,5-$DTBCH_2$ oxidation precedes in two steps: i) the first step is the fast step in which the catalyst binds to the substrate molecule in a reversible reaction to form [catalyst-substrate] intermediate. Binding the catalyst to

View Article Online
DOI: 10.1039/C9NJ06131B

the substrate renders the catalyst sensitive to react with O_2 and leads to formation of the ternary adduct [catalyst-substrate-O_2].

ii) The second step is the irreversible slow step where the ternary intermediate spontaneously converts to the oxidation product with releasing the catalyst in its original form. This step occurs slowly in successive stages to form the oxidation products, and therefore is the rate determining step. However, under anaerobic conditions this slow step was not achieved indicating the essential involvement of O_2 in the catalytic cycle.

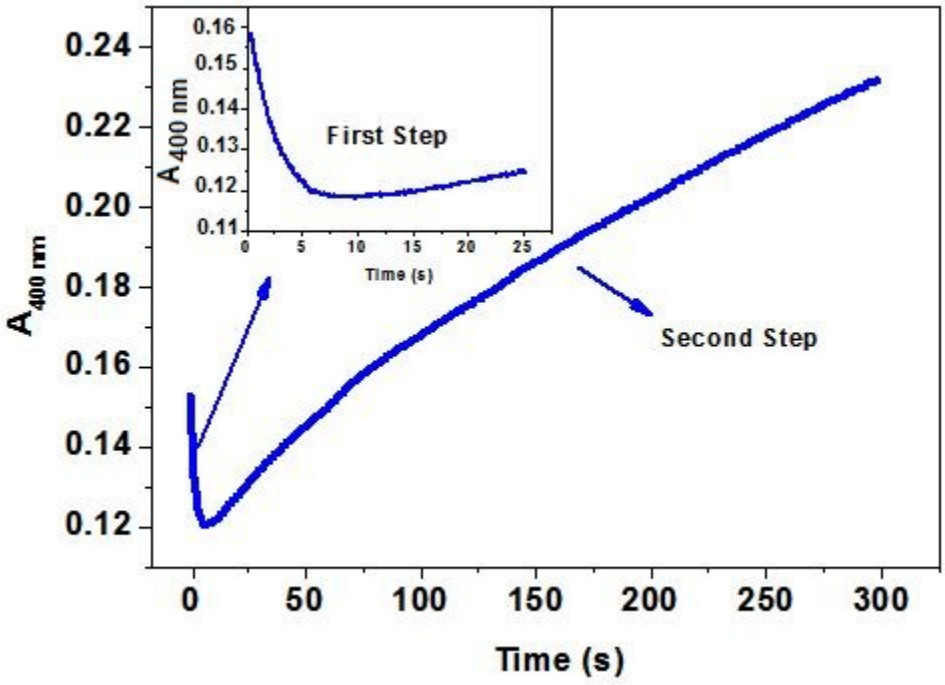

Fig. 8: Representative kinetic trace obtained by the stopped-flow spectrophotometry monitored at 400 nm for the reaction of complexes **1** with 3,5-DTBCH$_2$ in MeOH at 296 K

The initial rate method was used to treat the kinetics of current oxidation reactions by monitoring the characteristic band growth of the oxidation product. The reaction rate dependence on the concentration of the substrate was determined by the treatment of the catalyst solution (1×10^{-4} M) by substrate solutions with concentrations of 1×10^{-3} to 8×10^{-3} M. The obtained results are represented graphically by plotting the catalysis rate, k_{obs} versus the substrate concentration, [S] for the first and second steps as shown in Figures 9 and 10. On the other hand similar plots related to complex **2** and other substrates such as

View Article Online
DOI: 10.1039/C9NJ06131B

pyrocatechol, 4-methyl catechol and 4-nitro catechol are presented in the supplementary materials S11-S16.

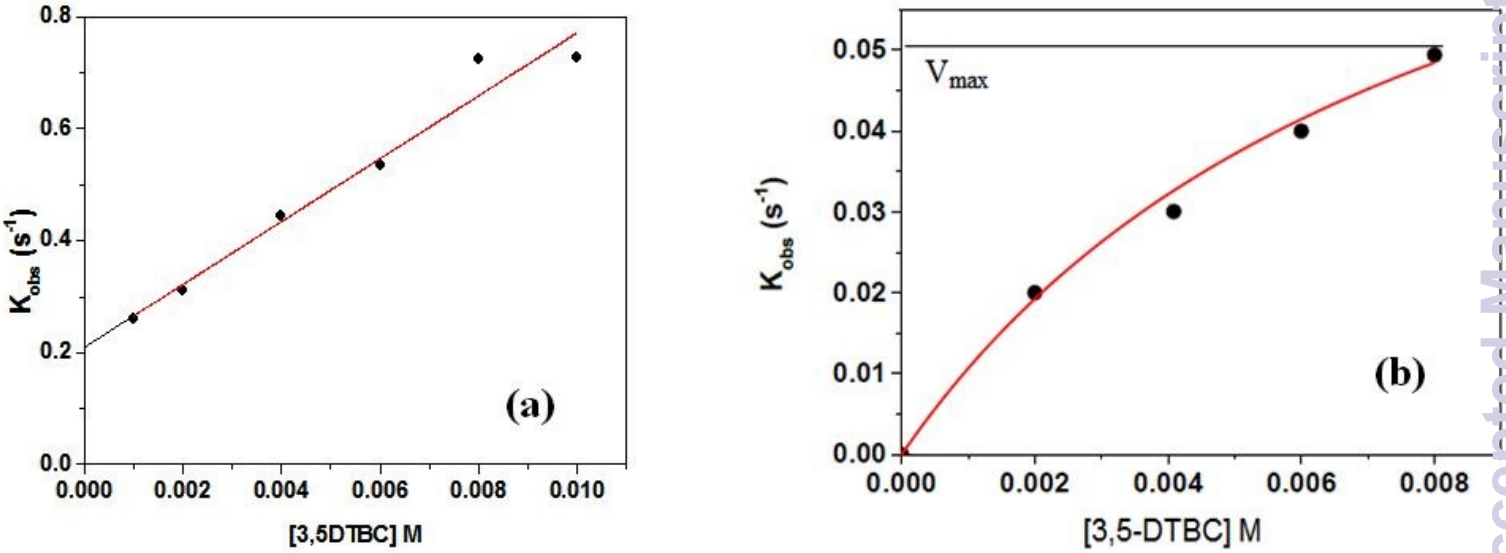

Fig. 9: Dependence of the initial rate on the concentration of the substrate for the oxidation reaction of 3,5-DTBCH$_2$ catalyzed by complex **1** in methanol; (a) is the first step and (b) is the second step.

Figures 9 and 10 show that at low substrate concentrations, the reaction rate (k_{obs}) changes linearly with [S], and indicates first-order behavior whereas at high concentrations of the substrate, k_{obs} becomes independent on [S] in reference to the kinetic saturation pattern. The simplest model explaining the running catalytic behavior is presented in equations 3 and 4, which corresponds to the Michael Menten method, where catalytic kinetic parameters such as V_{max}, k_{cat} and K_M are defined. Based on the plots of Michael Menten the computed data for the studied substrates are in the ranges of 50 - 490 s^{-1} for k_{cat}, and for K_M is 15 – 37 × 10^{-4} M, in the case of studied catechols and k_{cat} = 50 - 150 s^{-1}, and K_M = 20 – 29 × 10^{-4} M, for *o*-APH$_3$ (Table 11).

View Article Online
DOI: 10.1039/C9NJ06131B

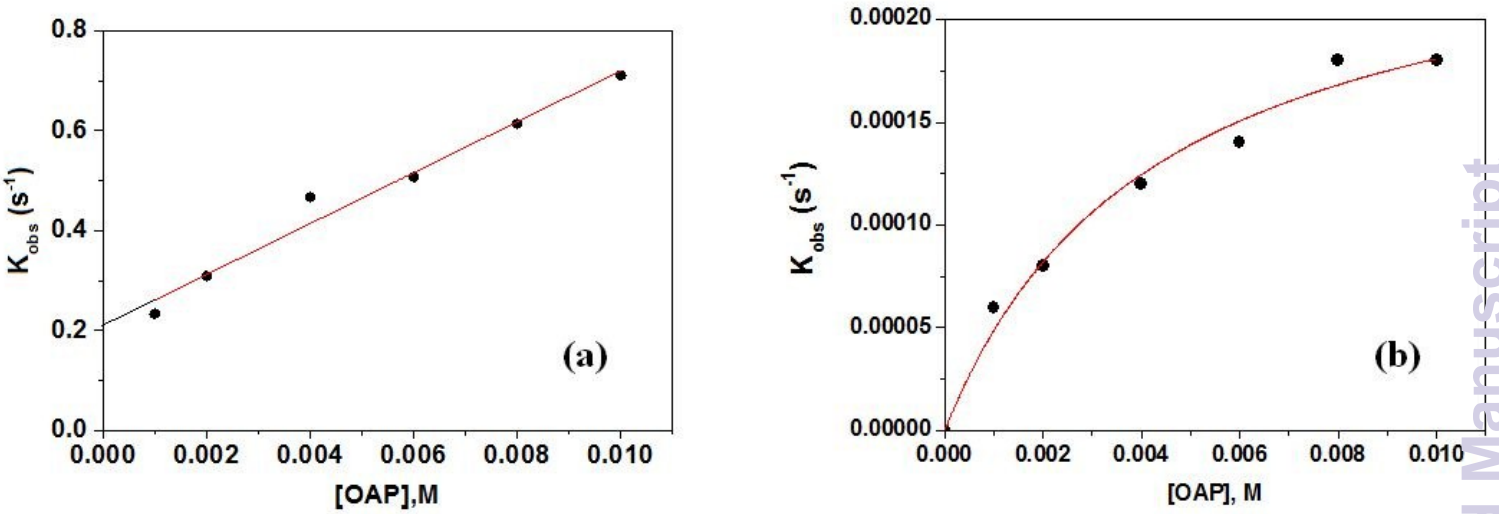

Figure 10: Dependence of the initial rate for on the concentration of the substrate for the oxidation reaction of *o*-APH_3 catalyzed by complex **1** in methanol; (a) is the first step and (b) is the second step. The concentration of complex was 1.0×10^{-4} M and the reaction was followed at 433 nm

For the reversible reactions 3 and 4 the equilibrium constant K_1 ($K_1 = k_1 / k_{-1}$), of the first step is a practical determination of the bonding affinity (coordination) of the studied substrates towards the current copper(II) complexes. Concerning 3,5-$DTBCH_2$ the corresponding K_1 values are 286 and 75 for complexes **1** and **2** respectively (Table 11). In the same context *o*-APH_3 exhibits binding affinity values of 243 for complex **1** and 89 in the case of complexes **2**. The difference in the coordination affinity of the studied substrates could be ascribed to structural causes. However, the values of K_M listed in Table 11 are in almost consistent with values of K_1 for both complexes **1** and **2**.

The ratio k_{cat}/K_M with a unit of M^{-1} s^{-1} is a useful index for description the catalytic efficiency and its values (Table 11) for complexes **1** is greater than **2** and the same trend holds for the binding affinity of these complexes towards the examined substrates. Previous studies for catechol oxidation by copper(II) catechol oxidase models reported that transfer of electrons from the catecholate ring to the copper(II) centers occurs only after the deprotonated catechol binds copper(II) centers [12]. In this context binding of the current functional models to the dibasic catecholate anion (3,5-$DTBC^{2-}$) or *o*-APH_2^- is the spark of the beginning catalytic oxidation cycle [1,34]. This is evident from the data in Table 11 which indicate that the catalytic efficiency of **1** and **2** depends on their K_1 values. The data in Table 11 show that both 3,5-$DTBCH_2$ and *o*-APH_3 exhibit binding

View Article Online
DOI: 10.1039/C9NJ06131B

affinity towards complex **1** greater than complex **2**. In the same vein, for the other substrates under study K_1 values follow the order: 4-NO_2-$CatH_2$ > 3,5-$DTBCH_2$ > *o*-APH_3 > $CatH_2$ > 4-Me-CaH_2 in the case of complex **1** (Table 11). The same order holds for the oxidase catalytic efficiency (k_{cat}/K_M) of complex **1** (Table 11) except in the case of 4-nitrocatechol.

The oxidation pattern of both pyrocatechol and 4-methy catechol continued as in the case of 3,5-$DTBCH_2$ and *o*-APH_3 and marked oxidation products were formed.

Concerning 4-nitro-catechol, its kinetic trace (S14) displayed only the fast step while the kinetically significant slow step is absent and no oxidation product formed.

Table 11: Catalytic kinetic parameters for oxidation of various substrates

Complex/substrate		k_1	k_{-1}	k_1/k_{-1}	V_{max} M s^{-1}	k_{cat} h^{-1}	$K_M \times 10^{-4}$ M	$k_{cat}/K_M \times 10^4$
	$CatH_2$	24	0.27	89	0.015	150	37	4.054
1	3,5 DTBC	56.2	0.209	268	0.049	490	29	16.896
	4-CH_3- $CatH_2$	19.2	0.369	52	0.008	80	15	5.333
	4-NO_2- $CatH_2$	98.2	0.104	944	-	-	-	-
	OAP	51.0	0.210	243	0.015	150	20	7.5
2	3,5 DTBC	30.9	0.409	75	0.0058	58	24	2.416
	OAP	34.1	0.384	89	0.005	50	29	1.724

Several dinuclear and mononuclear copper(II) complexes has been synthesized and used as a catalyst for the oxidation of the widely used substrate 3,5-$DTBCH_2$ [12,13,14,35,36]. A list of reported copper systems (catechol oxidase mimics) with their kinetic parameters of 3,5-$DTBCH_2$ oxidation are listed in Table 12. The data in Tables 11 and 12 show that the catecholase mimetic catalytic activity of the current copper(II) complexes are comparable with the other copper based catechol oxidase functional models. However, the efficiency of the native catechol oxidase enzyme is still the highest compared to all the functional models studied [37].

View Article Online
DOI: 10.1039/C9NJ06131B

Table 12: Copper based complexes showing catechol oxidase and phenoxazinone synthase mimetic activity with their important kinetic parameters

Complex	Substrate	k_{cat} (h^{-1})	K_M (M)	k_{cat}/K_M (M^{-1} h^{-1})	Ref.
$[CuL^1OH]ClO_4$	3,5-$TBCH_2$	21.0	10×10^{-4}	2.1×10^4	12b
$[CuL^1Cl]Cl$	3,5-$TBCH_2$	88.2	9.5×10^{-4}	9.2×10^4	12b
$[CuL^1](ClO_4)_2$	3,5-$TBCH_2$	15.0	10.0×10^{-4}	1.5×10^4	12b
$[Cu_2L^2](ClO_4)_2$	3,5-$TBCH_2$	172.0	9.2×10^{-4}	18.69×10^4	12b
$[CuLL'(H_2O)]NO_3$	3,5-$TBCH_2$	10.9×10^3	4.0×10^{-3}	2.8×10^6	13b
[CuLL"]ClO_4	3,5-$TBCH_2$	11.4×10^3	3.6×10^{-3}	3.1×10^6	13b
$[CuLL'(H_2O)]NO_3$	*o*-APH_3	2.1×10^3	5.6×10^{-3}	0.4×10^6	13b
[CuLL"]ClO_4	*o*-APH_3	2.1×103	7.5×10^{-3}	0.60×10^6	13b
$[CuL_2\ H_2O].Cl_2$	3,5-$TBCH_2$	8.65×10^3	4.08×10^{-3}	2.16×10^6	14
[CuLL' Cl].H_2O	3,5-$TBCH_2$	4.75×10^3	1.50×10^{-3}	3.10×10^6	14
[CuLL'].$2H_2O$	3,5-$TBCH_2$	1.84×10^3	1.50×10^{-3}	1.20×10^6	14
$[CuL_2\ H_2O].Cl_2$	*o*-APH_3	6.65×10^3	5.16×10^{-3}	1.22×10^6	14
[CuLL' Cl].H_2O	*o*-APH_3	8.33×10^3	1.47×10^{-3}	5.66×10^6	14
[CuLL'].$2H_2O$	*o*-APH_3	8.55×10^3	6.30×10^{-3}	1.35×10^6	14
$[Cu_2(L\text{-}(CH_3)_7)(N_3)_3]$	3,5-$TBCH_2$	2.88×10^4	7.0×10^{-4}	72.0×10^6	35
$[Cu_2(L^{98})_2(H_2O)]$	3,5-$TBCH_2$	265	20.2×10^{-3}	31.12×10^3	36
Catechol oxidase*	Catechol	8.25×10^6	0.0025	33.00×10^8	37

*Catechol oxidase from Ipomoea batatas (sweet potatoes).

In recent decades the modeling of phenoxazinone syntheses activity has been performed by small molecules enzyme mimics and few copper based complex was demonstrated as an active catalyst for both DTBC and OAP oxidation [12,13,14,35,36].

View Article Online
DOI: 10.1039/C9NJ06131B

However the present copper(II) oxidase models exhibit catalytic promiscuity towards the aerobic oxidation of both DTBC and OAP with catalytic efficiency analogous to the reported models as shown in Tables 11 and 12.

3.9. Electrochemical and energetic considerations

Direct interaction between the molecular oxygen and the organic substrates are spin forbidden reactions and this kinetic barrier can only be overcome in the presence of an appropriate catalyst [38]. Many mononuclear and binuclear copper complexes were involved in the oxidation of catechols via activation of O_2 [1]. The role of copper complex in this process is the medium to transfer a pair of electrons from the substrate molecule to O_2. In the case of *o*-APH_3 the copper(II) complexes job is one electron transfer from the *o*-aminophenolate (*o*-APH_2^-) to O_2.

The present stopped follow kinetic studies demonstrate that, the binding of dibasic catecholate anions or *o*-APH_2^- to copper(II) center is the initial step of the catalytic oxidation reactions. In this situation the pathway of electrons transfer is undoubtedly donor – acceptor interactions which proceed via the inner-sphere mechanism. The standard free energy for a bimolecular electron transfer reaction is then given by the relation [39]: $\Delta G^o = - n \times [E^o_{(acceptor)} - E^o_{(donor)}] \times 96.48$ kJ mol^{-1} V^{-1}

The stopped follow kinetic studies demonstrate that the overall reaction of the present catalytic oxidation processes proceed via formation of [catalytst/substrate/O_2] ternary complex rout. In this regard the rate determining step comprises two successive stages of the electron transfer reactions. In the case catechols the first oxidation stage implies transfer a pair of electrons from the catecholate ring to two copper(II) centers which results in the reduction of Cu^{II} to Cu^{I} and releasing the oxidation product *o*-quinone. Concerning *o*-APH_3 the first stage implies one electron movement from *o*-APH_3 to one catalyst molecule leading to reduction of Cu^{II} to Cu^{I} with concomitant formation the semioxidized intermediate *o*- aminosemiquinone (*o*-$APSQH_2$). In this situation the donor is the HOMO of *o*-APH_3 which has energy value greater than the LUMO of the acceptor (catalyst).

In the case of the catechols oxidation reaction the second stage implies binding O_2 to two Cu^{I} centers followed by two intramolecular electrons transfer from the two Cu^{I}

View Article Online
DOI: 10.1039/C9NJ06131B

centers to O_2 which results in the reduction of O_2 to H_2O_2 and the catalyst returns to its original active form. To determine the driving force for these electrons transfer reactions the redox potentials for the couples O_2/O_2^{2-} and $O_2/O_2^{\bullet-}$ are + 0.281 and – 0.33 V respectively were taken from literature [40]. Accordingly HOMO of copper(I) has a driving force (Table 10) that allows it to donate electrons to LUMO of O_2.

As regards *o*-APH_3 the produced intermediate, [*o*-$APSQH_2$-$Cu^{I}LL'$], reacts with the atmospheric oxygen to form the precursor [*o*-$APSQH_2$-$Cu^{I}LL'$-O_2]. An intramolecular electron-transfer from Cu^{I} center to O_2 leads to reduction of O_2 to the superoxide ($O_2^{\bullet-}$) fragment with concomitant formation of the ternary superoxo complex [(*o*-$APSQH_2$-$Cu^{II}LL'$)-O_2]. Thereafter, the superoxo complex can undergo several rearrangements that lead to the production of *o*-BQMI and H_2O_2 to close the catalytic cycle by releasing the original copper(II) complex.

Table 13: Electrochemical data (V) and free energy, ΔG^o (kJ mol^{-1} V^{-1}) of the catalytic aerobic oxidation of catechols to *o*-quinones and *o*-APH_3 to APX

Substrate	$E_{½}$ (V)	ΔG^o $2Cu^{2+}/2Cu^{+}$	ΔG^o O_2/O_2^{-}	ΔG^o O_2/O_2^{2-}
$CatH_2$*	0.3766	38.900		-96.48
3,5 DTBC	0.1200	−10.613		-96.48
4-CH_3- $CatH_2$*	0.3772	39.020		-96.48
4-NO_2- $CatH_2$*	0.6115	84.227		-96.48
o-APH_3	− 0.130	− 96.480	48.72	
Complex **1**				
3,5 DTBC		-8.683		-95.51
o-APH_3		-56.92	48.72	
Complex **2**				

*$E_{½}$ (V) values of $CatH_2$, 4-CH_3- $CatH_2$ and 4-NO_2- $CatH_2$ are taken from reference [40].

View Article Online
DOI: 10.1039/C9NJ06131B

The corresponding driving forces ($-\Delta G^{o}$) of the first stage in the case of 3,5 $DTBCH_2$ and *o*-APH_3 for complexes **1** and **2** lie between (− 96.480) and (−10.613) kcal mol^{-1} V^{-1}, while for the second stage in the case of catechols are in the range of -96.48 to – 95.51 kcal mol^{-1} V^{-1} (Table 13). The negative free energy values mean that these electron transfer (redox) reactions can spontaneously proceed. Therefore the current copper(II) complexes can perfectly drive the electrons transfer from the HOMO of the studied catechols to the LUMO of O_2. On contrary, the positive sign of ΔG^{o} values in the case of *o*-APH_3, where O_2 reduces to O_2^{-}, indicate that the first one-electron reduction of O_2 to give O_2^{-} is relatively unfavorable thermodynamically [41]. This discussion can justify the low catalytic efficiency of the studied copper complexes(II) toward the air oxidation of *o*-APH_3 compared to the corresponding catechols. In the same context the free energy (ΔG^{o} = 84.227 kJ mol^{-1} V^{-1}) of the electron transfer from 4-nitro catecholate ring to Cu^{II} is energetically unfavorable. Thus the aerobic catalytic oxidation process of 4-nitro catechol to the corresponding quinone was not completed.

3.10. Catalytic oxidation reactions in an inert atmosphere of N_2

To make sure participation of oxygen in the current catalytic oxidation processes, the catalytic oxidation reactions were carried out in an inert atmosphere of N_2. Under these conditions, the second step of the catalytic reaction cannot be observed as shown in Figure 11, indicating that the developing band is due to the formation of the quinone.

View Article Online
DOI: 10.1039/C9NJ06131B

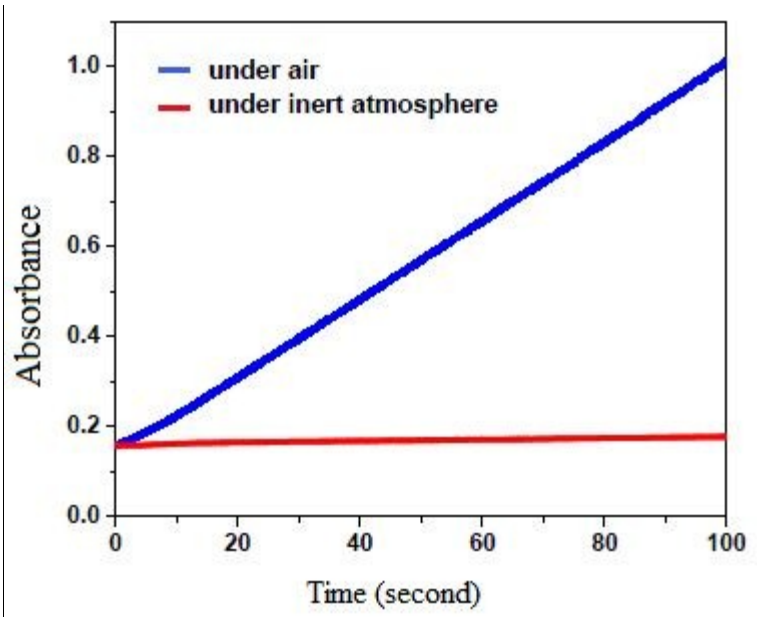

Figure 11: Representative kinetic trace obtained by stopped-flow spectrophotometry monitored at 400 nm for the reaction of complex **1** with 3,5-DTBC in the presence and absence of air in MeOH at 296 K

3.11. Detection of H_2O_2

Reaction of O_2 with the catalyst in presence of a substrate rarely generates H_2O and often leads to a reduction of oxygen to H_2O_2 with oxidation of catechol to *o*-quinone and *o*-APH_3 to *o*-BQMI. In order to confirm releasing of H_2O_2 as a by-product during the present catalytic oxidation reactions, oxidation of I^- to I_3^- by H_2O_2 was examined as described before [42]. Formation of I_3^- was detected by spectral monitoring the characteristic band of I_3^- at 353 nm as shown in Figure 12.

View Article Online
DOI: 10.1039/C9NJ06131B

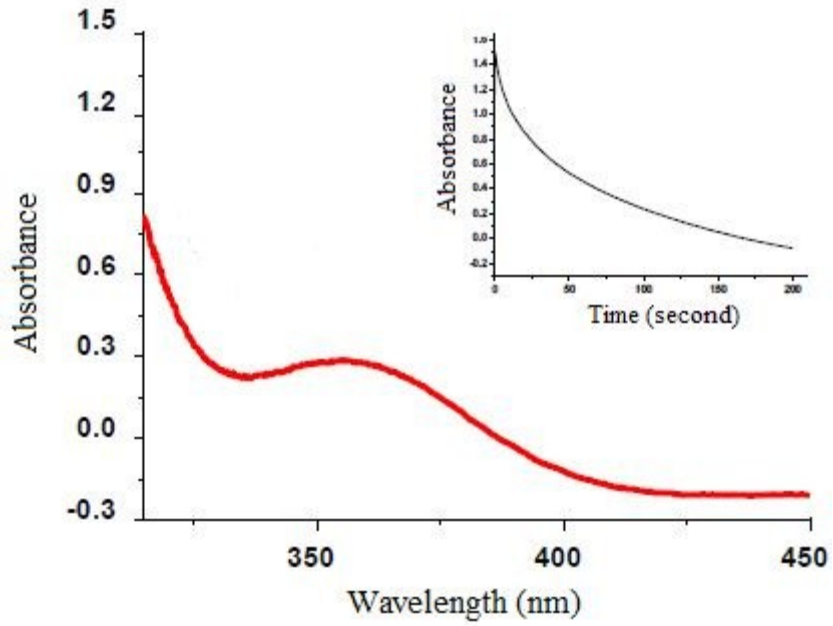

Figure 12: The electronic spectrum of I_3^- at 353 nm which formed by oxidation of I^- by action of H_2O_2 which released as a by product during the current catalytic oxidation of 3,5-DTBCH_2

3.10. Plausible catalytic reaction pathways

Spectral, electrochemical, and kinetic investigations have enhanced the proposed ping-pong mechanism of ongoing catalytic oxidation reactions. Catechol and *o*-APH_3 oxidation reactions by copper(II) complexes are thought to include reduction and oxidation cycle for copper(II) center as described below for both catechol (reactions 5 and 6) and *o*-APH_3 (reactions 7 and 8):

$$2Cu^{II} + CatH_2 \rightarrow Quinone + 2H^+ + 2Cu^{I} \quad (5)$$

$$2Cu^{I} + O_2 \rightarrow 2Cu^{II} + O_2^{2-} \xrightarrow{2H^+} 2Cu^{II} + H_2O_2 \quad (6)$$

$$Cu^{II} + o\text{-}APH_3 \rightarrow [o\text{-}APSQH\text{-}Cu^{I}] + H^+ \quad (7)$$

$$[o\text{-}APSQH\text{-}Cu^{I}] + O_2 \rightarrow [(o\text{-}APSQH\text{-}Cu^{II})\text{-}O_2] \quad (8)$$

$$[(o\text{-}APSQH\text{-}Cu^{II})\text{-}O_2] + H^+ \rightarrow [(o\text{-}APSQH\text{-}Cu^{II})\text{-}O_2H] \quad (9)$$

$$[(o\text{-}APSQH\text{-}Cu^{II})\text{-}O_2H] \rightarrow Cu^{II} + o\text{-}BQMI + H_2O_2 \quad (10)$$

In non catalytic reactions: *o*-BQMI + *o*-APH_3 → → → APX (11)

View Article Online
DOI: 10.1039/C9NJ06131B

Conclusion

The mixed ligand system 1,1′,4,4′-tetramethylethylenediamine (Me_4en) based and N-methyl iminodiacetic ($MIDAH_2$) or the ethylenediaminetetraacetic acid ($EDTAH_4$) were coordinated to copper(II) ion to form two ternary complexes **1** and **2**. Square pyramidal geometry was assigned to these copper(II) chelates based on comprehensive characterization by using a wide range of techniques including elemental analysis, electrochemical, X-ray, and other spectroscopic measurements. To better understand the catalytic activity of these complexes detailed kinetic studies were performed showing a different tendency of various phenols to oxidize and of the capability of these studied phenols to transform to the oxidation products, quinone or APX, is basically correlated with their binding affinity to complexes 1 and 2. As well, the nature of substituents on the catecholate ring affects the reduction potential of these phenols as shown in Table 13. In this regard, 3,5-$DTBH_2$ has bulky alkyl groups on the ring thus has low quinone-catechol reduction potential that makes it easily oxidized to 3,5-DTBQ. Although complexes **1** and **2** have convergent values of their redox potentials but complex **1** exhibits a remarkable higher catalytic activity as compared to complex **2**. This variation can be ascribed to the coordination affinity of the reported substrates. In the light of the above results, the factors affecting reactivity of the present copper(II) complexes and the propensity of oxidation of the studied phenols are mainly the substrate structure and the redox potential of both the metal complex and the concerned phenol. In addition to the driving force (λ) of the oxidation reaction or the free energy change ($-\Delta G^{o}$) associated with changes in the bond lengths and angles of the reactants, binding affinity of the concerned substrate towards the employed catalyst and flexibility of the geometrical changes of the catalyst during the catalytic cycle.

View Article Online
DOI: 10.1039/C9NJ06131B

References

[1] S. K. Dey and A. Mukherjee, Coord. Chem. Rev., 310 (2016) 80; and references therein

[2] J. Borovansky and P. A. Riley, Melanins and Melanosomes, Wiley-VCH Verlag & Co. KGaA, Boschstr, 12, 69469 Weinheim, Germany, (2011)

[3] J. Reedijk, Bioinorganic Catalysis, 1st Ed. Marcel Dekker, New York, (1993)

[4] E. I. Solomon, et al., Chem. Rev., 96 (1996) 2563; C. E. Barry, et al., Biochemistry, 28 (1989) 6323

[5] M. Le Roes-Hill, C. Goodwin S. Burton, Trends in Biotechnology, 27, 4 (2009) 248

[6] C. Gerdemann, C. Eicken, A. Magrini, H. E. Meyer, A. Rompel, F. Spener, B. Krebs, Bioch. Biophys. Acta., 1548 (1) (2001) 94

[7] C. Gerdemann, C. Eicken, A. Magrini, H. E. Meyer, A. Rompel, F. Spener, B. Krebs, Bioch. Biophys. Acta, 1548 (1) (2001) 94

[8] a) P. A.Vigato, S. Tamburini, L. Bertolo, Coord. Chem. Rev., 251 (2007)1311; b) V. G. Dave, P. J. Vyas, J. Curr. Chem. Pharm. Sc., 2 (2012) 133; c) H. Golchoubian, A.NematiKharat Polish, J. Chem., 79 (2005) 825; d) N. N. Murthy, M. Mahroof-Tahir, K. D. Karlin, Inorg. Chem., 40 (2001) 628; e) J. A. Drewry, P. T. Gunning, Coord. Chem. Rev., 255 (2011) 459; f) J. Reim, B. Krebs, J. Chem. Soc., Dalton Trans., (1997) 3793; g) K. S. Banu, T. Chattopadhyay, A. Banerjee, S. Bhattacharya, E. Suresh, M. Nethaji, E. Zangrando, D. Das; Inorg. Chem., 47 (2008) 7083; h) C Fernandes, A Neves, A. J. Bortoluzzi, A. S. Mangrich, E. Rentschler, B. Szpoganicz, E. Schwingel, Inorg. Chim. Acta, 320 (2001) 12; i) L. Gasque, V. Manuel Ugalde-Saldıvar, I. Membrillo, J Olguın, E. Mijangos, S. Berne, I. Gonzalez, J. Inorg. Biochem. 102 (2008) 1227

[9] a) S. Torelli, C. Belle, I. Gautier-Luneau, J. L. Pierre, E. Saint- Aman, J. M. Latour, L. Le Pape, D. Luneau, Inorg. Chem., 39 (2000) 3526; b) K. Abe, K. Matsufuji, M. Ohba, H. Okawa. Inorg. Chem., 41 (2002) 4461; c) L. Dubois, D.-F. Xiang, X.-S. Tan, J. Pecaut, P. Jones, S. Baudron, L. Le Pape, J. M. Latour, C. Baffert, S. Chardon-Noblat, M.-N. Collomb, A. Deronzier, Inorg. Chem., 42 (2003) 750

[10] a). Karsten, A. Neves, A. J. Bortoluzzi, M. Lanznaster, V. Drago, Inorg. Chem., 41 (2002) 4624; b) K. D. Karlin, J. C. Hayes, Y. Gultneh, R. W. Cruse, J. W. McKown, J. P.

View Article Online
DOI: 10.1039/C9NJ06131B

Hutchinson, J. Zubieta, J. Am.Chem. Soc., 106 (1984) 2121; c) C. J. O'Connor, D. Firmin, A. K. Pant, B. Ram Babu, E. D. Stevens, J. Am. Chem. Soc., 25 (1986) 2300

[11] J. A. Drewry, P. T. Gunning, Coord. Chem. Rev., 255 (2011) 459

[12] a) P. Gentschev, N. Moller, B. Krebs, Inorg. Chim. Acta, 300–302 (2000) 442; b) A. M. Ramadan, M. M. Ibrahim, I. M. El-Mehasseb, J. Coord. Chem., 65 (13) (2012) 2256; c) S. Y. Shaban, A. M. Ramadan, R. Van Eldik, J. Coord. Chem., 65 (14) (2012) 2415; d) I. A. Koval, P. Gamez, C. Belle, K. Selmeczi, J. Reedijk, Chem. Soc. Rev., 35 (2006) 81; e) S. Y. Shaban, A. M. Ramadan, M. M. Ibrahim, M. A. Mohamed, R. van Eldik, Dalton Trans., 44, (2015)14110; f) I. A. Koval, P. Gamez, C. Belle, K Selmeczi, J. Reedijk, Chem. Soc. Rev., 35, (2006) 814–840; h) C Belle, K Selmeczi, S. Torelli, J-L Pierre, C. R. Chimie 10 (2007) 271, i) A. M. Ramadan, M. M. Ibrahim, S. Y. Shaban, J. Mol. Struct., 1006 (2011) 348

[13] a) A. M. Ramadan, S. Y. Shaban, M. M. Ibrahim, F. I. El-Shami, S. A. Al-Harbi, J. Mol. Struct, 1189 (2019) 360; b) S. Y. Shaban, A. M. Ramadan, M. M. Ibrahim, F. I. El-Shami, R. van Eldik, Inorg. Chem. Acta 486 (2019) 608; c) A. M. Ramadan, S. Y. Shaban, S. M. E. Khalil, M. Shebl, R. A. S. El-Naem, J. Chin. Adv. Mater. Soc., 5 (2017) 215; d) R. Than, A. A. Feldmann, B. Krebs, Coord. Chem. Rev., 182 (1999) 211; e) L. I. Simandi, T. M. Simandi, Z. May, G. Besenyei, Coord. Chem. Rev., 245 (2003) 85; f) K. Selmeczi, M. Reglier, M. Giorgi, G. Speier, Coord. Chem. Rev., 245 (2003) 191; g) A. M. Ramadan, S. Y. Shaban, H. Eissa, Int. J. Adv. Res., 2, 8 (2014)116; h) A. M. Ramadan, Y. L. Aly, S. M. E. Khalil, M. Shebl, R A. S. El-Naem, Int. J. Adv. Res., 3, 7, (2015)10; i) A. M. Ramadan, S. Y. Shaban, M. M. Ibrahim, M. M. El-Hendawy, H. Eissa, S. A. Al-Harbi, J Chin. Chem. Soc., 67 (2020) 135

[14] A. M. Ramadan, S. Y. Shaban, M. M. Ibrahim, S. A. Sallam, F. I. El-Shami, S. Al-Juaid, J Mater Sci, 55 (2020) 6457

[15] SAINT, V6.02, Bruker AXS, Madison, WI, (1999)

[16] G. M. Sheldrick, SADABS, Area-detector Absorption Correction, (1996)

[17] W. J. Geary, Coord. Chem. Rev., 7 (1971) 81

[18] J. Coates, Interpretation of Infrared Spectra, A Practical Approach, Encyclopedia of Analytical Chemistry, R. A. Meyers (Ed.), Ó John Wiley & Sons Ltd, Chi Chester, (2000) 10815

View Article Online
DOI: 10.1039/C9NJ06131B

[19] K. Nakamoto. Infrared and Raman Spectra of Inorganic and Coordination Compounds, 3rd Edn., John Wiley and Sons Inc., New York (1978).

[20] J. Dehand, J. Jordanov, F. Keck, A. Mosset, J. J. Bonnet, J. Galy, Inorg. Chem., 18 (1979) 1543

[21] A. B. P. Lever, Inorganic Electronic Spectroscopy, 2nd ed., Elsevier, New York. (1984)

[22] a) O. O. E. Onawumi, O. O. P. Faboya,; O. A. Odunola, T. K.; Prasad, Pajasekharan, M. V. Polyhedron, 27, (2008) 113; b) R. N. Patel, N. Singh, D.K. Patel, V.L.N. Gundla, Indian J Chem., (2007) 422; c) N.M. El-Metwaly, I.M. Gabr, A.A. El-Asmy, Transition Met. Chem., 31 (2006) 71

[23] R. L. Dutta, A. Syamal, Elements of Magnetochemistry, 2nd Ed., Affiliated East-West Press, Delhi, (2007)

[24] I. Fidone, K.W.H. Stevens, Proc. Phys. Soc. London, 73 (1959) 116

[25] B. J. Hathaway, D. E. Billing, Coord. Chem. Rev., 5 (1970) 143

[26] B. J. Hathaway, R. J. Dudley, P. Nicholls, J. Chem. Soc. A, (1968) 1845

[27] a) M. A. Mahmoud, A. M. Abbas, S. A. Zaitone, A. M. Ammar, S. A. Sallam, J. Mol. Struct., 1180, (2019) 861; b) W. I. F. David, K. Shankland, L. B. Mccusker, C. H. Baerlocher, Structure Determination from Powder Diffraction Data, Oxford University Press Inc.: New York, (2002); c) D. M. Oliveira, W. N. Mussel, L. P. Duarte, G. D. F. Silva, H. A. Duarte, E. C. L. Gomes, L. Guimarães, S. A. V. Filho, *Quim. Nova*,. 35, 10 (2012) 1916

[28] A. Altomare, C. Cuocci, C. Giacovazzo, A. Moliterni, R. Rizzi, N. Corriero and A. Falcicchio, EXPO 2013: a kit of tools for phasing crystal structures from powder data, J. Appl. Cryst., 46 (2013) 1231

[29] G. M. Sheldrick, SHELX 2013, University of Gottingen, Germany, (2013)

[30] X.-H. Zhou, X.-Y. Le, L. Long, S. Chen, Chem. Res. Chinese U., 21 (2005) 119; A. Tovar-Tovar, J. C. Garcia-Ramos, M. Flores-Alamo, L. Ruiz-Azuara, Acta Cryst., E67 (2011) m1796.

[31] a) X. Le, S. Liao, X. Liu, X. Feng, J. Coord. Chem., 59 (2006) 985; b) D. Xu, A. Xie, Y. Xu, C. Zhang, W. Chen, J. Coord. Chem., 39 (1996) 273

View Article Online
DOI: 10.1039/C9NJ06131B

[32] M. D. P. T. Sotomayor, A. A. Tanaka, L. T. Kubota, Electro Chim. Acta, 48, (2003) 855

[33] a) A. B. Zaki, M. Y. El-Sheikh, J. Evans and S. A. El-Safty, Polyhedron, 19 (2000) 1317; b) J. Kaizer, R. Csonka and G. Speier, J. Mol. Catal. A: 180 (2002) 91.

[34] a) S. K. Dey, A. Mukherjee, Coord. Chem. Rev., 310 (2016) 80 and references therein; b) U. Hollstein, Chem. Rev., 74 (1974) 625; c) J. C. Freeman, P. G. Nayar, T. P. Belgely, J. J. Villafranca, Biochemistry, 32 (1993) 4826

[35] K. S. Banu, T. Chattopadhyay, A. Banerjee, S. Bhattacharya, E. Suresh, M. Nethaji, E. Zangrando, D. Das, Inorg. Chem., 47 (2008) 7083

[36] C. T. Yang, M. Vetrichelvan, X. Yang, B. Moubaraki, K. S. Murray, J. J. Vittal, Dalton Trans., (2004) 113

[37] C. Eicken, F. Zippel, K. Buldt-Karentzopoulos, B. Krebs, FEBS Lett., 436 (1998) 293

[38] a) A. Naqui, B. Chance, E. Cadenas, Ann. Rev. Biochem., 55, (1986) 137; b) W. S. Caughey, Biochemical and Clinical Aspects of Oxygen, Academic Press, New York, (1979)

[39] I. Bertini, H. B. Gray, E. I. Stiefel and J. S. Valentine, Biological Inorganic Chemistry Structure and Reactivity, University Science Books, USA, (2007)

[40] D. Nematollahi1, A. A. Taherpour, S. Jameh-Bozorghi, A. Mansouri, B. Dadpou, Int. J. Electrochem. Sci., 5 (2010) 867

[41] J. S. Valentine, C. S. Foote, A. Greenberg and J. F. Liebman, Active Oxygen in Biochemistry, Blackie Academic and Professional, An Imprint of Chapman and Hall, London, (1993)

[42] S. Sengupta, B. N. Mongal, S. Das, T. K. Panda, T. K. Mandal, Michel Fleck, S. K. Chattopadhyay, S. Naskar, J. Coord. Chem., 71, 8, (2018) 1